



Utrecht University

Masterthesis

Insights into Reaction Behaviours in Single Zeolite ZSM-5 Channel Orientations as Studied with *Operando* UV-Vis Spectroscopy

Inorganic Chemistry and Catalysis, Debye Institute for Nanomaterials Science, Utrecht University, Universiteitsweg 99, 3584 CG Utrecht, The Netherlands

Author: Onno van der Heijden, BSc
Daily supervisor: Donglong Fu, MSc
Supervisor: Prof. Dr. Ir. Bert M. Weckhuysen
Second supervisor: Dr. Florian Meirer

15-02-2019

Abstract

Zeolite ZSM-5 with an MFI framework, consisting of sinusoidal (*a*-axis) and straight (*b*-axis) channels, is a heavily utilised catalysts. This drives continuous research on understanding the structure-performance relationships. However, the role of each single zeolite channel orientation during chemical reactions has yet to be understood, due to the complex structures of the conventional zeolites. In this thesis, by rationally synthesising oriented crystals and thin-films with high (only) accessibility to sinusoidal or straight channels, the channel-performance relationships during oligomerisation reactions and alcohol-to-hydrocarbons processes was studied using a series of advanced characterisation techniques, *e.g.* *operando* UV-Vis Spectroscopy, Confocal Fluorescence Microscopy (CFM), X-ray Diffraction and NH₃-TPD. Firstly, *a*- and *b*-oriented zeolite ZSM-5 crystals, with high accessibility to sinusoidal and straight channels, respectively, were studied to decipher the product distribution and deactivating behaviours of the catalysts, showing faster deactivation of *a*-oriented crystals and a more pronounced aromatic cycle in *b*-oriented crystals. Furthermore, the knowledge obtained from the oriented crystals was confirmed on oriented zeolite ZSM-5 thin-films. First, larger molecules: 4-methoxystyrene and thiophene, that are also catalysed by zeolite ZSM-5 were studied, demonstrating that the *a*-oriented channel favours the formation of small molecules, while *b*-oriented channels promote the formation of extended molecules. Using *operando* UV-Vis diffuse-reflectance spectroscopy coupled with mass spectrometry the methanol-to-hydrocarbons process was monitored. It was demonstrated that small coke species are primarily formed in straight channels, while large coke species mainly cover the *a*-oriented surface. Meanwhile, toluene was observed in the effluent from the *a*-oriented channel, while MS data shows the absence of toluene in the effluent from the *b*-oriented channels. We speculate that, due to their tortuous structure, the formation of small coke species in the *a*-oriented channel is suppressed and toluene can diffuse out and further conjugates to large coke species on the external surface. We believe this work opens a new research approach to study heterogeneous catalysts.

Table of Contents

Abstract.....	1
List of Figures.....	4
List of Tables.....	5
1. Introduction	6
1.1 Zeolites.....	6
1.1.1 Zeolite structures	6
1.1.2 Applications	7
1.1.3 Zeolite ZSM-5.....	8
1.2 ZSM-5 Catalysed Reactions.....	9
1.2.1 4-methoxystyrene oligomerisation.....	9
1.2.2 Thiophene oligomerisation.....	10
1.2.3 Methanol-to-hydrocarbons	11
1.2.4 Ethanol-to-hydrocarbons.....	13
1.3 Research Methodology.....	14
2. Experiments & Methods	15
2.1 Synthesis of Oriented Zeolite Thin-Films and Crystals.....	15
2.1.1 Chemicals.....	15
2.1.2 Trimer tC6 (SDA) Synthesis.....	15
2.1.3 Synthesis of a-oriented MFI-seed crystals	16
2.1.4 Synthesis of oriented thin-films	17
2.1.5 Crystal synthesis.....	18
2.2 Characterisation Techniques	19
2.2.1 Scanning electron microscopy	19
2.2.2 X-ray diffraction.....	19
2.2.3 Temperature programmed desorption of ammonia	19
2.2.4 Reactions utilising operando/in-situ UV-Vis with online MS or GC.	20
2.2.5 Spectroscopic techniques on thin-films	20
2.2.6 Analysis of retained hydrocarbons with GC-MS	23
3. Reaction Behaviours Studied on Oriented Zeolite Crystals.....	24
3.1 Physiochemical Properties.....	24
3.2 Operando UV-Vis spectroscopic Studies of the Methanol-to-Hydrocarbons Process..	26
3.2.1 Deactivation behaviours and product distributions	26
3.2.2. Evolution of hydrocarbons studied with operando UV-vis spectroscopy.....	27
3.2.3. Study of retained hydrocarbons in the first reaction stage.....	27
4. Reaction Behaviours studied on Oriented Thin-Films	30

4.1 Fabrication of Oriented Zeolite Thin-Films	30
4.1.1 Synthesis of oriented zeolite seed crystals.....	30
4.1.2 Attachment of oriented zeolite monolayers	31
4.1.3 Growth of continuous zeolite thin-films.....	34
4.2 Oligomerisation Reactions	35
4.3 Alcohol-to-Hydrocarbons Processes on Zeolite ZSM-5 Thin- Films	37
4.3.1 Operando UV-Vis on oriented ZSM-5 thin-films	37
4.3.2 Ex-situ assessment of the location of the coke species.....	39
5. Conclusions & Outlook	41
5.1 Conclusions	41
5.2 Outlook.....	42
Acknowledgements	43
References.....	44

List of Figures

Figure 1.1 Applications of zeolites per weight in 2013, based on data from Janshekar et al. ¹⁷	7
Figure 1.2 3D ball and stick representations of the zeolite MFI framework with the grey atoms representing silica and the red atoms representing oxygen. Viewed along the (a) b-axis and the straight channels and along the (b) a-axis and sinusoidal channels.....	8
Figure 1.3 Schematic image of MFI zeolite channel system with the straight b-oriented channel from top to bottom and the sinusoidal a-oriented channel from left to right ⁶⁷	8
Figure 1.4 4-methoxystyrene oligomerisation products and their presence within zeolite ZSM-5 channels ²⁶	9
Figure 1.5 The mechanism of thiophene oligomerisation via two different pathways, a ring opening pathway (black arrows) and direct oligomerisation pathway (blue arrows), in acidic zeolite. Based on G. Whiting et al ⁹	10
Figure 1.6 Dual cycle mechanism of methanol conversion over ZSM-5 zeolites, showing the olefinic cycle on the left and the aromatic cycle on the right, as well as their interconnection, based on Olsbye et al ³⁸	12
Figure 1.7 Mechanistic description of the production of small olefins in the Ethanol-to-Hydrocarbons process, adapted from Chowdhury et al ⁶⁰	13
Figure 1.8 Full overview of the synthesized crystals and films as used in this thesis, including the crystals and thin-film samples and the ZSM-5 pore system as studied.	14
Figure 2.1 Trimer TPAOH (tC6), used as SDA for the synthesis of a-oriented seeds and crystals.	16
Figure 2.2 Schematic image of the probed channels (red) in oriented ZSM-5 thin-films by x/y polarised light.	20
Figure 2.3 Bypass setup for operando MTH on thin-films, containing an UV-vis probe and on-line MS.	21
Figure 2.4 Fixed bed operando setup for MTH synthesis with an UV-vis probe and on-line GC used for oriented crystals.	22
Figure 3.1 SEM images of (a) a- and (b) b-oriented ZSM-5 crystals, with Si/Al ratio = 125 and their respective (b, e) XRD pattern and (c, f) particle sizes.....	24
Figure 3.2 NH ₃ -TPD profile of (a) a-oriented 125 and (b) b-oriented ZSM-5 crystals with Si/Al = 125	25
Figure 3.3 The conversion (a, c) of a- and b-oriented ZSM-5 in MTH synthesis at 350 °C with a WHSV of 5 h ⁻¹ , in c the graphs are shifted based on the data point with the highest conversion, to compare the deactivation slope. The (b) ethylene/C5 olefins and (d) ethylene/propylene are given, showing the relative propagation of the olefin and aromatic cycle and the ratio of the essential MTO products respectively.....	26
Figure 3.4 Operando UV-vis of (a) a- and (b) b-oriented ZSM-5 Crystals in their first 1.5 minutes of MTH reaction at 350 °C with a WHSV of 5 h ⁻¹	27
Figure 3.5 Ex-situ UV-vis of a- and b-oriented ZSM-5 crystals after (a) 3 and after (b) 10 minutes respectively.....	28
Figure 3.6 GC results of the products extracted from (a) a-oriented ZSM-5 and (b) b-oriented ZSM-5 crystals after 3 minutes of MTH synthesis.....	29
Figure 4.1 SEM image of purely siliceous (a) a- and (b) b-oriented MFI crystals, used as seed crystals for monolayers synthesis.....	30
Figure 4.2 (a) Monolayers containing plenty of empty space after spin coating, (b) monolayer spin-coated with epoxy with a poor packing, (c) high amount of out of plane crystals after spin coating, (d) high amount of out of plane crystals after double spin-coating.	32
Figure 4.3 SEM images of a- and b-oriented monolayers MFI seed crystals on a (PEI coated) quartz substrate, with the accordingly measured XRD.	33
Figure 4.4 SEM images of (a, b) a- and (d, e) b-oriented thin-films after secondary growth in a SGM with Si/Al ratios of (a, d) 125 and (b, e) 45 with a representative XRD spectrum of (c) a-oriented ZSM-5 and (f) b-oriented ZSM-5 respectively.	34
Figure 4.5 UV-Vis spectra of (a, b) 4-methoxystyrene and (c, d) thiophene oligomerisation on oriented thin-films, showing the (a) presence of the trimeric carbocation in green and its (b) absence in red. ..	35

Figure 4.6 (a) Tilt series of a-oriented zeolite ZSM-5 thin-film with Si/Al = 125 after 4-methoxystyrene oligomerisation. (b) Ex-situ UV-Vis of b-oriented ZSM-5 and a-oriented ZSM-5 thin-films after 4-methoxystyrene oligomerisation.	36
Figure 4.7 (a, b) Methanol-to-hydrocarbons and (c, d) ethanol-to-hydrocarbons on oriented thin-films during the first 3 minutes of reaction with the probed channel being depicted on the left and the assigned molecules depicted inside the spectra, which are active HCP species, coke precursors and external coke.	38
Figure 4.8 (a) MS spectrum after 1200 seconds showing toluene present in the effluent of a-oriented thin-films, but not in the effluent of b-oriented channels. (b) The proposed model based on the presence of toluene in the effluent of a- and absence from b-thin films.	38
Figure 4.9 Confocal fluorescence microscopy image of oriented thin-films with Si/Al = 125 excited by a 561 nm laser (top), as a flat substrate and with a 30° tilt on a stage (bottom). In the red box an example of the kind of coke species probed by the 561 nm laser is given.	39
Figure 4.10 Ex-situ comparison of oriented thin-films as flat substrates compared to a 30- and 45-degree angle. The images next to the spectra, show the orientation of the thin-film when the substrate is flat.	40

List of Tables

Table 3.1 Particle size distributions as measured from the SEM image.	25
Table 3.2 Acid site density of a- and b-oriented ZSM-5 as calculated by NH ₃ temperature programmed desorption.	25
Table 4.1 a-oriented monolayer synthesis techniques used in literature.	31
Table 4.2 Attempted parameters for coating of polymer (PEI) on top of a glass/quartz substrate.	33
Table 4.3 Assignment of the UV-Vis absorption peaks for 4-methoxystyrene oligomerisation.	35
Table 4.4 Assignment of the UV-Vis absorption peaks for thiophene oligomerisation.	36
Table 4.5 Assignment of the UV-Vis absorption peaks in methanol-to-hydrocarbons reactions.	37

1. Introduction

1.1 Zeolites

Zeolites (aluminosilicates) were discovered by the Swedish chemist Axel Cronstedt in 1756¹, who named them zeolites (to boil (zeo) and stone (lithos) in Greek) after their apparent boiling when heated¹. They can either be formed naturally by volcanic activity or be synthesised in the lab². Up to this point, 245 different zeolite frameworks have been recognised by the International Zeolite Association (IZA)³. They are widely applied in the petrochemical industry for e.g. fluid catalytic cracking, alkylation and methanol to hydrocarbons (MTH) synthesis due to their unique properties, such as angstrom scale pores, Brønsted acid sites and high stability⁴.

1.1.1 Zeolite structures

Zeolites consist of tetrahedrally coordinated silica and alumina. These species can form a multitude of zeolitic building blocks, which can be combined into a vast amount of frameworks, of which the most commonly industrially applied are the big five : FER, MFI, MOR, BEA and FAU². Common characteristics among these materials are high stability, micro porosity and Brønsted acidity⁴, which makes them suitable for catalysis².

Brønsted acidity is obtained when a tetravalent silicon atom is exchanged for a trivalent aluminium atom⁵. This exchange results in a negative framework charge, which can be compensated by a hydrogen atom, providing the desired Brønsted acid site⁶. Besides their acidity, the channel system of these zeolites is essential for catalysis. They consist mostly of, possibly intersecting, 8, 10 or 12 membered ring (MR) channels or cages with windows. In multi-dimensional channel systems the intersections of these channels might be essential, as they often have a slightly larger diameter, providing space for bulkier transition states⁷. The combination of the size and shape of the channels and intersections, result in three forms of shape selectivity: product, reactant or transition state⁸. The product and reactant shape selectivity are determined by the possibility of diffusion of either the reactant or product in and out of the zeolites' microporous channels. Whereas transition state shape selectivity is determined by the possible accommodation of the transition state within either the pores or intersections⁹, either promoting the formation of a transition state or suppressing it.

On a larger, industrial scale, zeolites are mostly used in the form of extrudates. However they can also be grown in oriented thin-films. These membranes or thin-films are promising for both separation¹⁰ and catalysis¹¹. The orientation of these thin-films can be grown, with the help of oriented crystals, along a certain channel^{12,4}. This can be done by synthesising a monolayer of purely siliceous oriented crystals followed by secondary growth¹³. These oriented thin-films can also be used, as well-defined model systems for catalytic reactions.

1.1.2 Applications

The total amount of zeolites used can be separated into two categories: natural and synthetic. Approximately 60% of the total use are natural zeolites, they are used as feed additives, in construction, for water treatment and for environmental uses¹⁴. However, they are not abundantly used in catalysis, so they will not be further discussed here. Synthetic zeolites, on the other hand, are used in a large multitude of industrial syntheses, including fluid catalytic cracking, hydrocracking, isomerisation and methanol-to-hydrocarbons synthesis¹⁵. Their main use, however, is as detergents (28% of total zeolite consumption by weight), as well as desiccants (5% of total zeolite consumption by weight)¹⁶ with a total of 1.817 million tons produced in 2013¹⁷ (overview in Figure 1.1). The most abundantly used zeolite in catalysis is zeolite Y, as the main component of the fluid catalytic cracking (FCC) catalyst¹⁸.

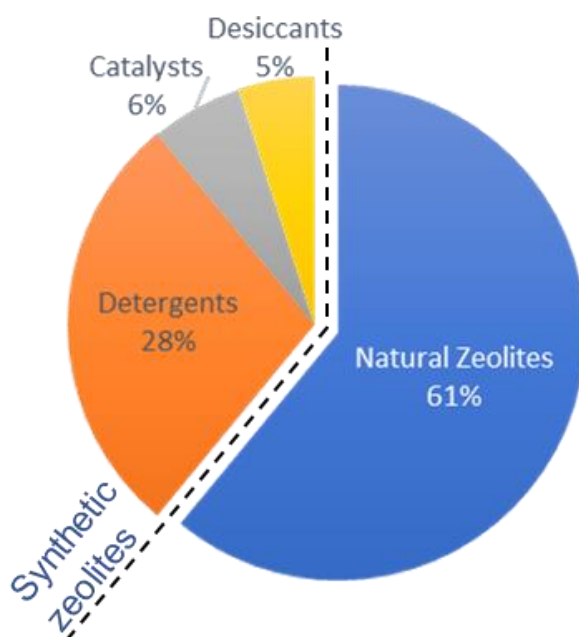


Figure 1.1 Applications of zeolites per weight in 2013, based on data from Janshekar et al.¹⁷

The FCC catalysts are built up from a multitude of materials, with as major component zeolite Y¹⁹, providing the acid sites as well as the desired product selectivity towards the major components of gasoline, as well as propylene¹⁹. Besides that, there is silica and alumina present to produce a matrix of meso- and macroporosity, providing access and facilitating the pre-cracking of larger molecules¹⁹. All those components are held together in a clay. The second most important industrial process catalysed by a zeolite is hydrocracking. The main catalyst used for this process is similar to the FCC catalyst consisting of the identical faujasite (FAU) framework, although this zeolite Y has usually been dealuminated¹⁶. Besides that, another hydrogenation function is added to the zeolite, this is either a promoted transition metal sulphide or a noble metal, such as platinum or palladium¹⁶. For isomerisation and alkylation, zeolites with the desired product selectivity are chosen. Zeolite ZSM-5 (MFI) is used for the isomerisation of xylene²⁰, ferrierite (FER) for the isomerisation of olefins²¹ and mordenite (MOR) for naphtha isomerisation²¹. For the methanol-to-hydrocarbons (MTH) synthesis, both ZSM-5 (MFI) and SAPO-34 (CHA) are used. These will be further discussed in the section concerning the MTH reaction (Chapter 1.2.3).

1.1.3 Zeolite ZSM-5

Zeolite ZSM-5, first patented by scientists at ExxonMobil in 1972²², has a 3-dimensional MFI framework, which has an orthorhombic unit cell with: $a = 20.09 \text{ \AA}$, $b = 19.75 \text{ \AA}$ and $c = 13.14 \text{ \AA}$. In Figure 1.2, two cross sections of the MFI framework are shown, one through the (1.2a) b -oriented channel and the other through the (1.2b) a -oriented channel. In ZSM-5 a certain amount of silicon atoms can be replaced by aluminium atoms, resulting in Brønsted acidity as described before.

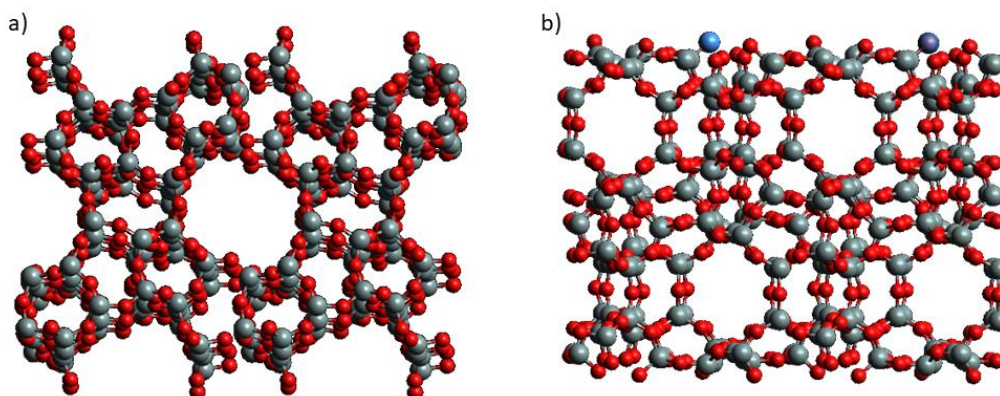


Figure 1.2 3D ball and stick representations of the zeolite MFI framework with the grey atoms representing silica and the red atoms representing oxygen. Viewed along the (a) b -axis and the straight channels and along the (b) a -axis and sinusoidal channels.

The ZSM-5 zeolite has 2 accessible medium sized 10-membered ring channels: a straight channel running through the b -axis and a sinusoidal channel running through the a -axis, as shown in Figure 1.3. The dimensions of these channels are $0.54 \times 0.56 \text{ nm}^2$ and $0.51 \times 0.55 \text{ nm}^2$ for the sinusoidal and straight channels respectively²³. The intersections of the channels, provide a slightly larger space, allowing for bulkier transition states to be formed²⁴. The combination of these properties results in the shape selectivity, as induced by the framework. Even though the ZSM-5 zeolite has been used extensively in industry and academia, a complete understanding of the actual properties, such as the reaction behaviours of the separate channels, has yet to be cleared up.

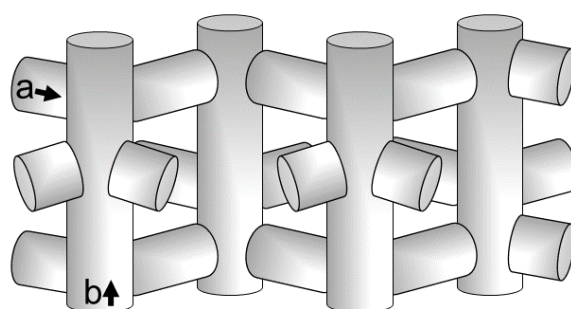


Figure 1.3 Schematic image of MFI zeolite channel system with the straight b -oriented channel from top to bottom and the sinusoidal a -oriented channel from left to right⁶⁷.

1.2 ZSM-5 Catalysed Reactions

ZSM-5 can catalyse a multitude of reactions in industry. In this thesis we focus on the alcohol-to-hydrocarbons reaction, because of its relevance to a more sustainable planet. Additionally, two probe reactions with larger reactant molecules, thiophene and 4-methoxystyrene oligomerisation, have been investigated to extend our knowledge gained to molecules of various sizes.

1.2.1 4-methoxystyrene oligomerisation

The oligomerisation of 4-methoxystyrene is catalysed by the intrinsic Brønsted acidity of ZSM-5. The monomer gets protonated, after which dimers and trimers can form²⁵. It was earlier reported that due to the MFI channel structure, the bulkier trimeric carbocation only forms in the straight *b*-oriented channel, whereas the dimeric carbocation is observed in both channels²⁶ (as shown in Figure 1.4). The formed products exhibit absorption at 585 and 630 nm for dimeric and trimeric carbocations respectively^{25,27}. Resulting in molecules suitable for spectroscopic analysis with UV-Vis absorption and fluorescence measurements.

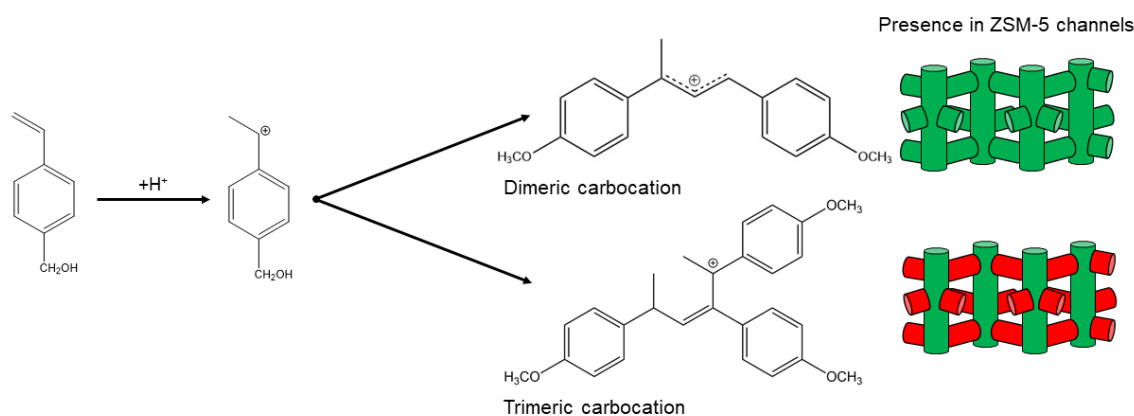


Figure 1.4 4-methoxystyrene oligomerisation products and their presence within zeolite ZSM-5 channels²⁶.

1.2.2 Thiophene oligomerisation

Another probe reaction applied on the acidic zeolite is thiophene oligomerisation. First, a protonated monomer is formed, followed by consecutive oligomerisation reactions, which occurs either by direct oligomerisation or via a ring opening pathway²⁸. The complete mechanism, as proposed by G. Whiting et al.²⁹, is given below (Figure 1.5). The products formed during the reactions can be used as a probe for the zeolite pores, as the reaction is relatively straight forward as well as highly space selective inside the zeolite. The absorbance of UV-light by the reaction products is dependent on the length of the oligomer, as larger carbocations, with a more delocalised π -system, absorb at higher wavelengths. Therefore, the UV-Vis absorption wavelength increases with oligomer growth (red-shift)³⁰.

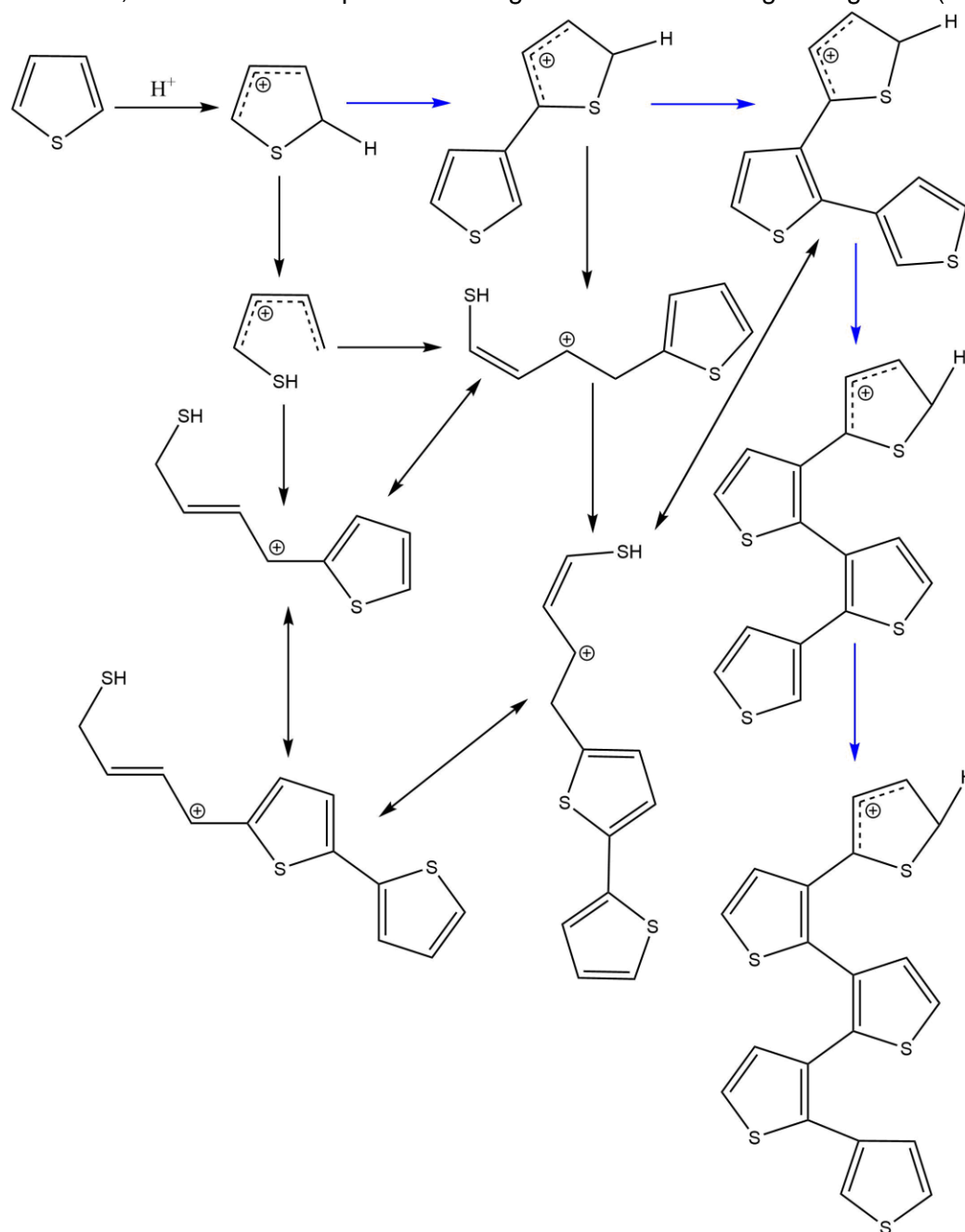


Figure 1.5 The mechanism of thiophene oligomerisation via two different pathways, a ring opening pathway (black arrows) and direct oligomerisation pathway (blue arrows), in acidic zeolite. Based on G. Whiting et al.²⁹.

1.2.3 Methanol-to-hydrocarbons

The methanol-to-hydrocarbons (MTH) synthesis was first developed in 1977 by scientists at Mobil³¹, shortly after their discovery of zeolite ZSM-5. It provides a pathway to produce hydrocarbons from methanol, depending on the catalyst used and the reaction parameters. In literature multiple abbreviations are used for methanol conversions with different desired products, e.g. MTH (general), MTO (methanol-to-olefins), MTP (methanol-to-propylene) and MTG (methanol-to-gasoline).

Due to decreasing availability of crude oil and the fight against global warming, the industrial methanol-to-hydrocarbons synthesis has regained popularity³². As the oil reserves decline and the CO₂ concentration steadily increases, a less environmentally harmful approach is warranted. This is possible by converting the methanol into chemical building blocks from different feedstocks, like biomass and waste³³. When those feedstocks are in low supply, methanol is also available from natural gas and coal. Therefore, it provides either a green or alternative approach to produce liquid fuels, as well as plastics. Recently the largest industrial plant to date started operating in China, with a production capacity of 833,000 metric tons from coal as feedstock³⁴. They produce mainly propylene for acrylonitrile for clothing and fabrics, high performance polymers, hard hats and several different plastic products³⁴.

The synthesis is generally catalysed for industrial use by either SAPO-34 or ZSM-5 zeolites. These materials show a good olefins selectivity, combined with good stability. Especially SAPO-34 showed an incredible selectivity towards light olefins³⁵, although it is susceptible to faster deactivation³⁶. This zeolite consists of a CHA framework with cages of 10 x 6.7 x 6.7 Å³, having windows of 3.8 x 3.8 Å²,³⁷ containing the aromatic cycle products within those cages, while allowing reactants and products to flow in and out. Compared to the three-dimensional channel framework of ZSM-5, with intersecting straight and sinusoidal channels of 0.54 x 0.56 nm² and 0.51 x 0.55 nm², respectively, allowing for increased mobility of the HCP species. Due to more facile diffusion in a 3-D framework, the deactivation of ZSM-5 is much slower, compared to SAPO-34³⁷.

The mechanism of the MTH reaction is not universally the same and is dependent on the zeolite in which it is catalysed. The transition state selectivity is very different for small to big pore zeolites, as well as in cages with specific windows. The general consensus on the reaction mechanism of MTH over ZSM-5, which is studied here, is that it operates via a dual-cycle mechanism³⁸. This mechanism consists of an aromatic cycle, as well as an olefinic cycle (Figure 1.6). In the olefinic cycle mainly propylene, butylene and higher olefins are formed, compared to majority ethylene and some propylene being produced in the aromatic cycle³⁹. This provides an opportunity to tune the product selectivity by promoting one cycle over the other.

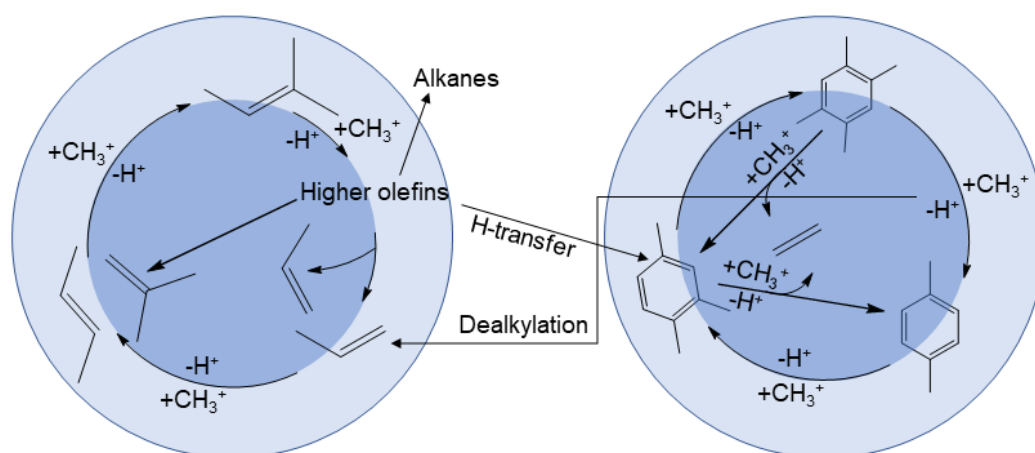


Figure 1.6 Dual cycle mechanism of methanol conversion over ZSM-5 zeolites, showing the olefinic cycle on the left and the aromatic cycle on the right, as well as their interconnection, based on Olsbye et al³⁸.

The parameters influencing the propagation of a certain cycle are: silica to alumina ratio, crystallite size, methanol space velocity, reaction temperature and co-feeding of HCP species⁴⁰. A high acid site density (low silica to alumina ratio), allows for multiple reaction steps to happen in fast succession, contributing to the aromatisation of longer olefins. This results in the propagation of the aromatic cycle over the olefinic cycle³¹. While a low alumina content provides an ideal catalyst to promote the formation of propylene⁴¹, thus a faster propagation of the olefinic cycle. The crystallite size influence is proposedly based on the longer residence time of methylbenzenes inside the zeolite pore system. This allows for multiple methylation and dealkylation reactions, producing ethylene, before exiting the crystal, thus promoting the aromatic cycle²³. With the methanol (or DME) space velocity decreasing, the olefinic cycle gets suppressed, while the aromatic cycle is promoted. This is caused by the promotion of the H-transfer reaction, resulting in aromatics, due to a longer contact time. In contrast to a decreasing contact time at a high space velocity, which promotes the olefinic cycle⁴². At increasing temperature, the aromatic cycle gets suppressed, due to the lack of chain carriers. Also, at 450 °C higher olefins are more likely to undergo cracking and desorption, instead of aromatisation, which decrease the amount of aromatics, thus suppressing the aromatic cycle⁴³. Co-feeding of certain HCP molecules can also influence the propagation of their respective cycle. The co-feeding of propylene does enhance the olefinic cycle⁴³, however, the co-feeding of higher olefins promote neither of the cycles. Supposedly, due to increasing both olefinic species, as well as the H-transfer of these species towards aromatics, balancing the increased propagation of both cycles⁴³. The co-feeding of aromatics does clearly promote the propagation of the aromatic cycle and thus increases the ethylene selectivity⁴⁴. Another influence on the propagation of a certain cycle is the channel in which the reaction takes place. The ZSM-5 straight and sinusoidal channels will influence the propagation of a specific cycle, as their size and shape can limit both the formation and the diffusion of important HCP molecules.

Although it has been heavily debated, the deactivation of the ZSM-5 catalyst seems to be caused by both external and internal coke species, formed as a side reaction to the HCP mechanism⁴⁵. The external coke, often large multiring aromatics or even graphene like sheets, block the diffusion in and out of the crystal³⁹. Thus resulting in a deactivated catalyst. Small coke species block the channels internally, blocking the active sites, as well as the diffusion through the channel. The hydrocarbons species build-up inside the zeolite framework could even lead to expansion of the framework over a specific axis, which can be observed with XRD⁴⁶.

1.2.4 Ethanol-to-hydrocarbons

As a similar reaction to methanol-to-hydrocarbons (MTH), ethanol-to-hydrocarbons (ETH) can be further explored as a sustainable process for liquid fuels and plastics. Ethanol's current main use is as a blend component in regular fuels, based on fossil resources. However, in the United States the production of ethanol is likely to rise above the blending need and ethanol as a separate fuel is unpractical⁴⁷. This requires a process that would use the more biofriendly ethanol to produce liquid fuels of a higher grade. This process could be ETH, providing a green route to actual gasoline length hydrocarbon species. Making it a reasonable addition to the MTG process, where biomass can be converted to gasoline via methanol.

Fundamentally, ETH is less well researched compared to MTH. What is known, is that the process provides a largely similar product distribution³⁹. A minor difference would be the existence of more ethyl substituted benzenes within the zeolite channels for the ETH process⁴⁸. The synthesis is also generally catalysed by similar zeolite materials, mainly ZSM-5⁴⁹. Mechanistically, however, the ETH process does not have an olefin cycle and operates by a single aromatic cycle⁵⁰. The olefins are produced from the homologation reaction of carbon-carbon bond couplings. This means that the formation of ethylene is mechanistically decoupled from the hydrocarbon pool, as shown in Figure 1.7⁵⁰.

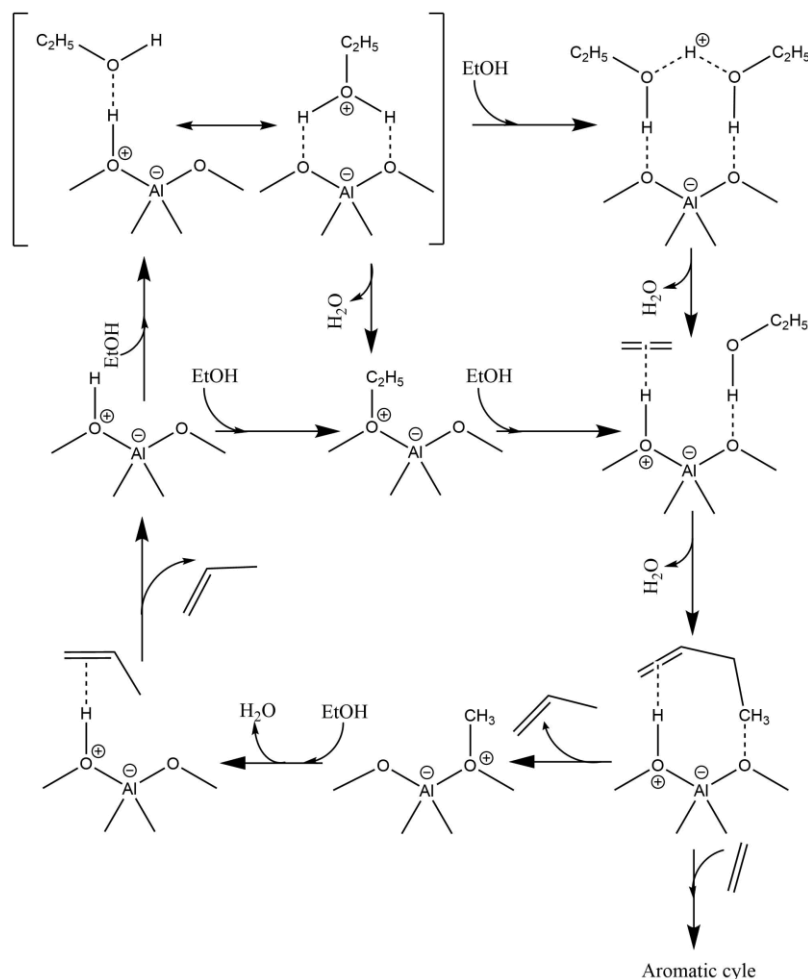


Figure 1.7 Mechanistic description of the production of small olefins in the Ethanol-to-Hydrocarbons process, adapted from Chowdhury et al⁵⁰.

1.3 Research Methodology

The aim of the thesis is to understand the specific role of single zeolite ZSM-5 channel orientations during chemical reactions. To this end, both oriented zeolite crystals and thin-films were synthesised and studied using a series of *operando*(in-situ)/*ex-situ* techniques during the methanol- and ethanol-to-hydrocarbons processes, as well as oligomerisation reactions.

In chapter 3, oriented crystals were synthesised and the deactivating behaviours and product distributions of these crystals during the MTH process were investigated. The crystal morphologies and crystallinities were measured with SEM and XRD, respectively. The evolution of hydrocarbons in the crystals and product distributions were monitored using *operando* UV-Vis coupled with GC. It should be pointed out that, due to their uniform crystallographic orientations, *a*- and *b*-oriented crystals have high accessibility to *a*-channels (sinusoidal) and *b*-channels (straight), respectively. After the reaction the trapped hydrocarbon species will be studied by dissolving the crystals in HF, extracting them into an organic layer and further analysis by GC-MS.

Furthermore, the reaction behaviours in single zeolite channel orientation were explored in oriented thin-films in chapter 4. On these thin-films in-situ 4-methoxystyrene and thiophene probe reactions were performed, while being characterised in-situ by an UV-Vis probe. The oligomerisation reactions provide information on channel specific behaviour, as certain products specifically form inside a single ZSM-5 channel^{26,51}, based on their respective shape selectivity. The reactivity of the different channels in the oriented thin-films during the industrially relevant Methanol-to-Hydrocarbons (MTH) was thoroughly explored. To this end characterisation methods e.g. Confocal Fluorescence Microscopy (CFM) and UV-Vis diffuse reflectance spectroscopy coupled with online MS were applied. These techniques provide specific information on the aromatics inside channels perpendicular to the incoming beam for the thin-films. This, combined with the orientation of the as-synthesised thin-films, will provide information about the reaction behaviours within a single ZSM-5 channel orientation.

By combining the insights obtained by the oriented crystals and thin-films during and after methanol-to-hydrocarbons, as well as the probe reactions (Figure 1.8). Further insight into the specific properties and reaction behaviours of the sinusoidal *a*-oriented and straight *b*-oriented zeolite ZSM-5 channel will be obtained.

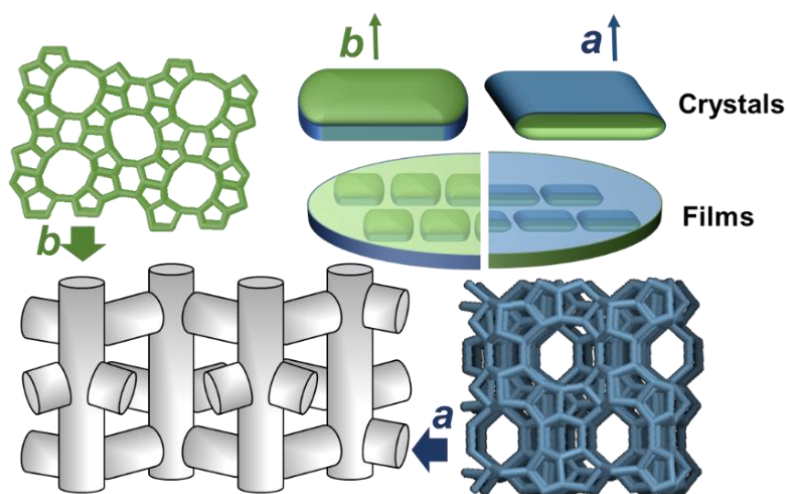


Figure 1.8 Full overview of the synthesized crystals and films as used in this thesis, including the crystals and thin-film samples and the ZSM-5 pore system as studied.

2. Experiments & Methods

2.1 Synthesis of Oriented Zeolite Thin-Films and Crystals

2.1.1 Chemicals

Branched polyethylenimine (PEI, Mw = 25000, Mn 10000, Sigma-Aldrich), sodium silicate solution ($\text{Na}_2\text{O}(\text{SiO}_2)_x \cdot x\text{H}_2\text{O}$, ~10.6% Na_2O , ~26.5% SiO_2 , Sigma-Aldrich), tetraethylorthosilicate (TEOS, 99%, Sigma-Aldrich), tetra-n-propylammonium hydroxide (TPAOH, 35 w%, Alfa Aesar), bis(hexamethylene)triamine, 1-iodopropane, 2-butanone, aluminium sulphate hexadecahydrate ($\text{Al}_2(\text{SO}_4)_3 \cdot 18 \text{H}_2\text{O}$, 98%, Sigma-Aldrich), hydrogen peroxide (30 wt.% in water, Sigma-Aldrich), ammonium nitrate (99%+, Acros Organics), ethanol (anhydrous, absolute, Biosolve), sodium fluoride (analytical grade, Merck), thiophene (GC standard, Sigma-Aldrich), methanol (99.8 %, Sigma-Aldrich), sulfuric acid (95%, reagent grade, Fischer scientific), potassium hydroxide pellets (KOH, 85%, Alfa Aesar), quartz plates (LSP Quartz B.V., 20 mm in diameter), glass plates (VWR, 22 mm in diameter)

2.1.2 Trimer tC6 (SDA) Synthesis

Trimer TPA (tC6) was reported as the structure directing agent for *a*-oriented MFI crystals. The synthesis was adapted from literature, described by Bonilla et al.⁵². Here bis(hexamethylene)triamine was alkylated with 1-iodopropane. Typically, 450 mL of 2-butanone, an excess of 72.6 g anhydrous potassium carbonate, HI and water scavenger, and 27.87 g of bis(hexamethylene)triamine were added to a three neck 1L round bottom flask. A dropping funnel and reflux condenser were connected to the flask. The round bottom flask was in a silicone oil bath on a stirring plate, flushed with nitrogen and vented from the top of the condenser. The solution was heated to 85 °C under nitrogen atmosphere. Afterwards 101 mL of 1-bromopropane was added dropwise with an dropping funnel. The reaction was conducted overnight (~15 hours), followed by filtration to remove 2-butanone. The recovered solids contain the target product, trimer-TPA³⁺3I⁻, along with impurity salts. The solids were dissolved in 100 mL of ethanol for several hours, followed by filtration. An off-white solid with a small amount of impurity was obtained by removing the ethanol with a rotary evaporator. Purification was performed by dissolving in 250 mL of cold 2-butanone again, after which an equal volume of ethyl acetate was slowly added to precipitate the product. After 10 hours the residue was removed from the solution by filtration. Higher purity of the target product can be obtained by repeating the washing steps, e.g. ethanol extraction and recovery by ethyl acetate. The purity was checked by ¹³C NMR (figure 2.1).

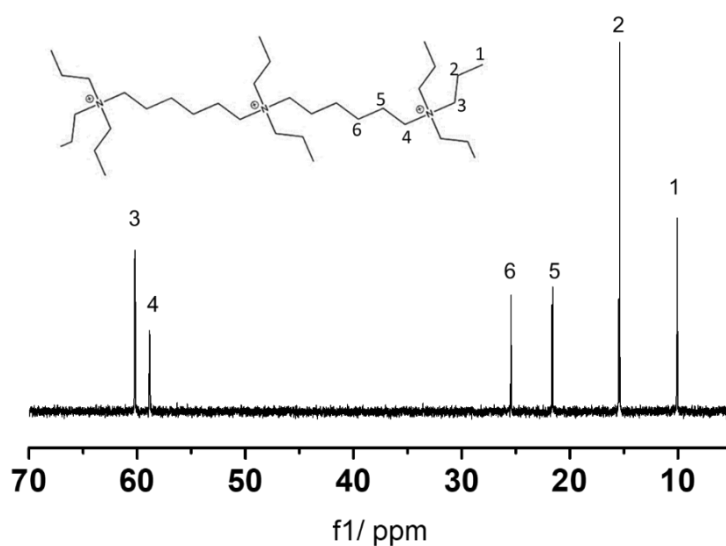


Figure 2.1 Trimer TPAOH (tC6), used as SDA for the synthesis of *a*-oriented seeds and crystals.

2.1.3 Synthesis of *a*-oriented MFI-seed crystals

For the synthesis of the *a*-MFI-seed crystals, t-C6, KOH, TEOS and miliQ water with a ratio of 1:5:8:1900 were added and stirred overnight. The solution was then poured into an autoclave through a filtration paper. The autoclave was placed in the (rotational) oven for 24 hours at 175 °C. The suspension was centrifuged for 1 minute at 4000 rpm. Washed twice with miliQ water followed by centrifuging at 4000 rpm again. Finally, the crystals were redispersed in acetone, after which they were centrifuged (4000 rpm, 1 minute), decanted and dried at 80 °C.

2.1.4 Synthesis of oriented thin-films

a-oriented monolayers were manually assembled on quartz plates after surface modification by dip-coating in polyethylenimine (PEI). Prior to dip-coating, quartz plates (20 mm in diameter) were submerged in 30 wt.% H₂O₂ for at least 45 minutes to clean the surface. The glass or quartz plates were placed into a 0.425 wt.% PEI solution for 2 minutes, with shaking simultaneously. Then the plates were dried by placing them into static air for 20 minutes at 60 °C. The *a*-oriented crystals were adhered to the substrate by a manual assembly method with latex gloves to prevent any contaminations⁵³. The monolayers were calcined at 550 °C to remove the organic layers, with a heating and cooling ramping rate of 1.5°C/min to 550 °C, and 2 hours at 550 °C.

b-oriented thin-films were fabricated by manual assembly, directly applied to the quartz plates (after H₂O₂ treatment) without surface modification, after which they were placed into static air at 175 °C for at least 1.5 hours to enhance the monolayer strength.

For secondary growth, a solution of sodium silicate solution (Na₂O(SiO₂)_y·yH₂O, ~10.6% Na₂O, ~26.5%SiO₂), EtOH, Al₂(SO₄)₃·18H₂O, H₂SO₄ and miliQ water with a molar ratio of 1SiO₂ : 1.5EtOH : xAl₂(SO₄)₃·18H₂O : 0.1825H₂SO₄ : 200 miliQ water was used, with x being adjusted for the desired Si/Al ratio. For thin-films with Si/Al = 45 Na₂SO₄ was added with a molar ratio of 0.1 with respect to sodium silicate above. This solution was made in two separate flasks, one with sodium silicate, miliQ water and EtOH and the other with Al₂(SO₄)₃·18H₂O, H₂SO₄ and miliQ water. These were magnetically stirred for 15 minutes, after which they were combined. The final solution was stirred for an additional 30 minutes. The monolayers (both *a*- and *b*-oriented) were vertically placed in a specially designed holder inside a Teflon lined 20 mL autoclave, into which the solution was added. The autoclaves were placed into static air for 24 hours at 175 °C. After reaction, the autoclave was removed from the oven and quenched by immersion in tap water. The as-synthesised zeolite thin-films were carefully removed and washed with copious amounts of miliQ water and dried at 80 °C. The plates were then calcined with a similar program as described above.

Finally, amorphous silica layer etching and ion exchange were conducted by ammonium fluoride and ammonium nitrate respectively. First, the thin-films were submerged in 0.2 M aqueous NH₄F solution for 1 hour. After which the sodium fluoride was removed, and the plates were washed with miliQ water. For ion exchange the thin-films were submerged into a 1M (NH₄)(NO₃) solution for at least 4 hours at 60 °C. After which the ammonium nitrate was removed and the plates were washed with miliQ water. Finally, they were dried and calcined with a similar procedure as described for *a*-oriented monolayers above, to obtain the H-form thin-films.

2.1.5 Crystal synthesis

Oriented zeolite crystals were prepared, largely based on literature methods^{4,52}. The synthesis solution of the *a*-oriented crystals consists of the ratios of 0.75 tC6, 620 MiliQ water, 1.17 KOH, 6 TEOS, whereas for the *b*-oriented crystals the solution consists of the following ratio : 0.9 TPAOH, 620 MiliQ water, 6 TEOS. The solutions were stirred for 4 hours. Consequently, $\text{Al}_2(\text{SO}_4)_3 \cdot 18\text{H}_2\text{O}$ was added, in the amount which would result in the desired Si/Al ratio. Thereafter, the solution was stirred for another hour before being transferred into a Teflon lined autoclave, which was then placed inside the oven at 175 °C with constant rotation.

After a reaction time of 24 hours, the autoclaves were removed from the oven and quenched with tap water. The formed suspensions were transferred to centrifugal tubes and MiliQ water was added. The suspensions were centrifuged at 3500 rpm for 3 minutes, decantated and redispersed in miliQ water. This was reproduced at least 3 times, followed by adding acetone and centrifuging one last time. The acetone was decantated and the crystals were dried at 80 °C. These dried crystals were then placed into the calcination oven, in which they were calcined at 550 °C to remove the organics, with a heating and cooling ramping rate of 2.2 °C/min to 550 °C, and at least 4 hours at 550 °C.

Finally, the obtained oriented ZSM-5 crystals were activated, by stirring overnight inside a 1 M ammonium nitrate solution at 80 °C to obtain the nitrate form. These crystals were washed with just water for at least three times, following a similar centrifuge and redispersion protocol. After drying, the calcination, following a similar program as described above, resulted in the final H-form product.

2.2 Characterisation Techniques

2.2.1 Scanning electron microscopy

The morphology of the as-synthesized seed layers, ZSM-5 thin-films and crystals were examined by scanning electron microscopy (SEM, Phenom ProX, Philips), operating at an acceleration voltage of 5 kV.

2.2.2 X-ray diffraction

X-ray diffraction (XRD) was used to study the orientation and crystallinity of the zeolite crystals and thin-films. Diffraction patterns were collected using a Bruker 2D phaser (2nd Gen) instrument, using a Cobalt radiation source, $\text{Co } \alpha = 1.789 \text{ \AA}$. The samples were rotated at 15 revolutions/min.

2.2.3 Temperature programmed desorption of ammonia

Temperature programmed desorption of ammonia (NH_3 -TPD) was performed on a Micromeritics Autochem II 2920 equipped with a TCD detector. Typically, 100 mg of oriented crystal was first degassed in He for 1 hour at 600 °C with a heating ramp of 10 °C/min. Thereafter, ammonia was absorbed at 100 °C until saturated, followed by flushing with He for 120 min. The ammonia desorption was monitored using the TCD detector until 600 °C with a ramp of 10 °C/min, using a He flow of 25 mL/min.

2.2.4 Reactions utilising operando/in-situ UV-Vis with online MS or GC.

To probe the reaction behaviour of these reactions, in-situ and *operando* spectroscopic techniques were utilised. The advantage of these techniques is that the information obtained is time-resolved⁵⁴. For *operando* spectroscopy, this information is obtained from both a spectroscopic technique, as well as GC or MS to study the effluent. So, that the formation of molecular intermediates inside the catalyst, can be combined with the product distribution in real-time²⁷. In-situ spectroscopy, on the other hand, probes a reaction by just a spectroscopic technique, in this case UV-Vis diffuse reflectance spectroscopy.

2.2.5 Spectroscopic techniques on thin-films

These previously described principles of in-situ and *operando* spectroscopy can also be applied on oriented thin-films. An additional tool, is the polarisation of the incoming UV-Vis light, not exciting molecules that have a dipole moment perpendicular to the polarisation of light⁵¹. Combined with the orientation of the pores in the as-synthesised thin-films, only channels parallel to the polarisation of light will show absorption. For the ZSM-5 thin-films that is the channel that is perpendicular to the orientation of the thin-film, so the *b*-oriented straight channels are probed in *a*-oriented thin-films and vice versa, as shown in red in Figure 2.2. This allows for channel specific information, inside the channel structure of zeolite thin-films, if the light absorbing molecules are aligned with the pore. So aromatic hydrocarbon pool species, as well as larger aromatics/coke species, formed inside a unique channel, can be successfully detected by this technique, which is essential for studying the channel specific reaction behaviour of zeolites. However, products from the olefin based cycle cannot be detected, as they are not aligned to a pore and do not absorb in the UV-Vis wavelength region.

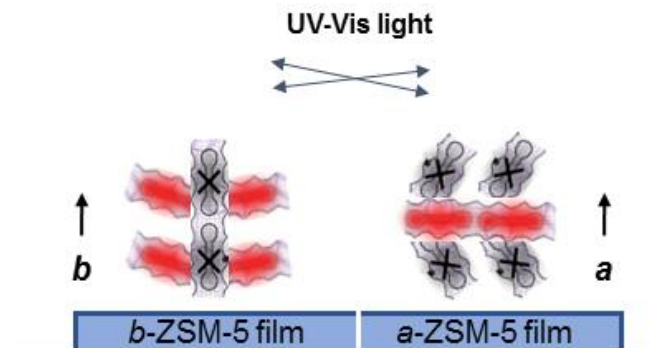


Figure 2.2 Schematic image of the probed channels (red) in oriented ZSM-5 thin-films by x/y polarised light.

For thiophene oligomerisation the probe was focused on the as-prepared thin-film while heated to 130 °C in an open Linkham cell. A single drop (a few μL) of thiophene was put on the oriented thin-film on the focused spot from the probe with a needle. After which it reacted for approximately 60 minutes, with spectra being taken every 15 seconds.

For the 4-methoxystyrene oligomerisation reaction an open Linkham cell was used together with the UV-Vis probe. The thin-films were placed in the Linkham cell, which was heated to 90 °C. A small droplet of 4-methoxystyrene was then placed on top of the thin-film on the UV-Vis probe's focus spot, with a needle. After which the reaction ran for 1 hour, while spectra were taken every 15 seconds. The reaction was, also performed with a 4-methoxystyrene flow. Using a bubble and a bypass system, 4-methoxystyrene was brought into the gas phase and lead over the oriented thin-films, while monitored in-situ by an UV-Vis probe.

For UV-Vis diffuse reflectance microscopy on MTH synthesis, a calcined thin-film after synthesis, secondary growth, etching and ion-exchange was used. The reaction was performed in a Linkham cell exclusively used for MTH reactions. Consisting of a gas inlet connected to a bypass system on a nitrogen line and an outlet connected to MS (Figure 2.3), with a heating stage on which the thin-film was placed. The cell was cleaned prior to reaction with SiO_2 catalyst grains at 500 °C under nitrogen flow (15 mL/min) for at least 30 minutes (checked for contaminations in MS). After cleaning, the thin-films were placed on the heating stage and heated to 350 °C. The probe was focused on the thin-film with a small tilt, and a reference and dark spectrum were taken prior to the synthesis. The reaction was initiated when the oxygen peak was stable (only the oxygen still present within the nitrogen flow). After which the direction of the flow was changed from the bypass through the methanol saturator. The MTH reactions were run for 90 minutes, while UV-Vis and MS spectra were measured continuously.

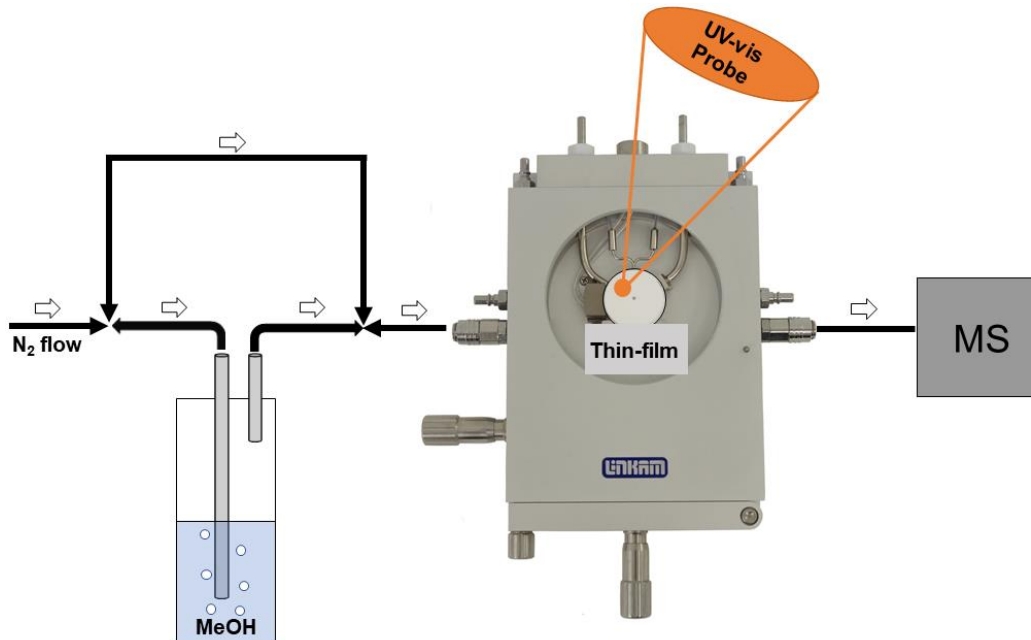


Figure 2.3 Bypass setup for *operando* MTH on thin-films, containing an UV-vis probe and on-line MS.

For UV-Vis during MTH a microscopy setup was used as well. Then the thin-film was placed in the cell facing the microscope (15x reflectance lens). The setup for MTH remains the same for probe to the microscope setup, but higher resolution in the UV region could be reached with the probe compared to the UV-diffuse reflectance microscope.

For the methanol-to-hydrocarbons *operando* reactions on crystals, a different and more advanced setup was used. It consists of a water bath to keep the methanol at a constant temperature, a quartz fixed bed reactor with 100 mg of catalyst, an oven around the reactor, an UV-Vis probe focused on the catalyst and a GC to analyse the effluent (Figure 2.4). The crystals were placed inside and calcined in cell at 550 °C under oxygen flow, with a heating ramp of 5 °C/min was used. The reaction was performed with a helium flow, with a WHSV of 5 g⁻¹ at 350 °C.

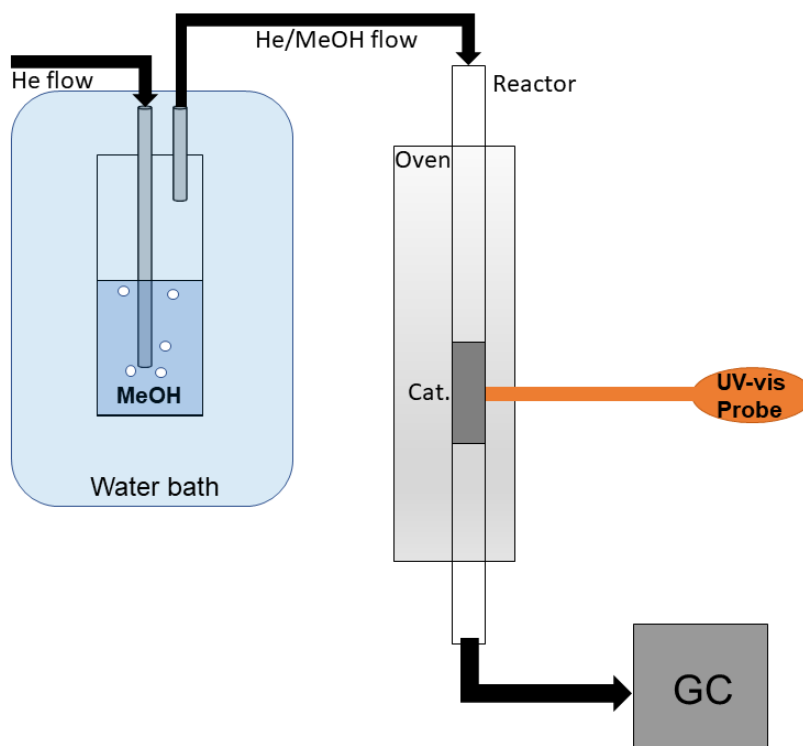


Figure 2.4 Fixed bed *operando* setup for MTH synthesis with an UV-vis probe and on-line GC used for oriented crystals.

From the GC data obtained, the conversion was calculated as follows:

$$\text{Conversion (\%)} = \frac{[\text{MeOH}_{in}] - [\text{MeOH}_{out}]}{[\text{MeOH}_{in}]} \quad (1)$$

The selectivity to hydrocarbons was calculated as a fraction of the consumed methanol, as follows:

$$\text{Selectivity (\%)} = \frac{n[\text{C}_n\text{H}_m]}{[\text{MeOH}_{in}] - [\text{MeOH}_{out}]} \quad (2)$$

2.4.5 Confocal fluorescence microscopy (CFM)

For CFM probe reactions were performed ex-situ. Here 15 μL of 4-methoxystyrene was put on small pieces of thin-film. They reacted for 1 hour at 80 $^{\circ}\text{C}$ inside a sample vial. The samples were measured after the reaction was completed. The images were taken while being focussed either on the bottom or the top of the sample, showing both intensity over the entire image as well as a spectrum within a certain spot.

For CFM studying MTH, the thin-films were reacted 1.5 hours at 350 $^{\circ}\text{C}$ with a 15 mL/min N_2 flow through a saturator, which is the same reaction as monitored by *operando* UV-Vis and MS as described before. These reacted samples were kept in a centrifugal tube wrapped with parafilm and were measured ex-situ.

The second setup is on a substrate, where the thin-film can be applied either under a 30-, 45- or 60-degree tilt. Here, tilt series were also recorded where the focus was changed to include the entire screen, in focus by changing the height of the sample. This technique allows to observe the channel, which is normally invisible under a perpendicular angle.

2.2.6 Analysis of retained hydrocarbons with GC-MS

Hydrocarbons trapped inside the post-reacted crystals after MTH reaction were analysed by dissolving the material in hydrofluoric acid, followed by extracting the hydrocarbons using CH_2Cl_2 . Typically, 50 mg of spent oriented ZSM-5 crystals was dissolved in 2 mL of hydrofluoric acid (45%) in a Teflon container with cap stirring for 1 hour. Then the organic compounds were extracted two times from the water phase by dropwise addition of 3 mL of CH_2Cl_2 . After 30 minutes, the organic phase containing the hydrocarbons was extracted from the bottom. Finally, 3 mL of saturated boric acid was added to the extracted organic solution to remove the HF residue. The solutions were separated again before filtering into GC-vials. Analysis of the extracted phase was performed on a Shimadzu GCMS-QP2010 GC/MS system, equipped with an Agilent VF-5 ms column as well as ESI-MS (Agilent, 1100 Series LC/MSD Trap).

3. Reaction Behaviours Studied on Oriented Zeolite Crystals

The crystal morphologies and crystallinities were measured with SEM and XRD, respectively. The evolution of hydrocarbons in the crystals and the product distribution were monitored using *operando* UV-Vis coupled with GC. It should be pointed out that, due to their uniform crystallographic orientations, *a*- and *b*-oriented crystals have high accessibility to *a*-channels (sinusoidal) and *b*-channels (straight), respectively.

3.1 Physiochemical Properties

The oriented crystals were synthesised as described in the experimental section. To confirm if the properties of the as-synthesised crystals correlate to the envisaged model systems: scanning electron microscopy (SEM), ammonium temperature programmed desorption (NH₃-TPD) were applied. These techniques provide information about the *a*- and *b*-orientation, morphology, crystallite size and acid site density.

The Phenom ProX, Philips SEM was used to image the oriented crystals. From these images the crystal length and morphology can be observed. As well as the presence of crystal intergrowths, defects and amorphous materials. The as-synthesised *a*- and *b*-oriented crystals with Si/Al ratio 125 are shown in Figure 3.1. Besides that, the XRD spectra of both crystals are given, in addition to their size, as measured from the SEM images (50 counts each).

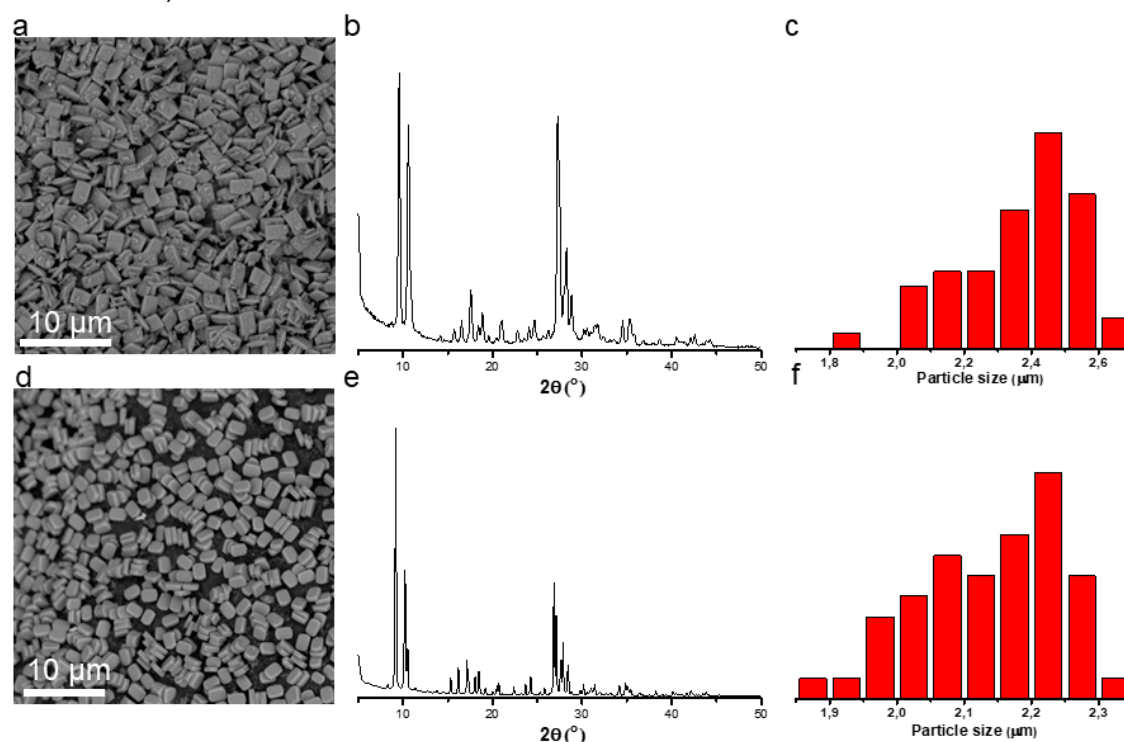


Figure 3.1 SEM images of (a) *a*- and (b) *b*-oriented ZSM-5 crystals, with Si/Al ratio = 125 and their respective (b, e) XRD pattern and (c, f) particle sizes.

The sizes over all their axes are given in Table 3.1 with their respective standard deviation.

Table 3.1 Particle size distributions as measured from the SEM image.

Sample	a-axis (μm)	b-axis (μm)	c-axis (μm)
a-oriented ZSM-5	0.55 ± 0.07	1.42 ± 0.11	2.36 ± 0.18
b-oriented ZSM-5	1.43 ± 0.08	0.66 ± 0.05	2.13 ± 0.10

To probe the acidity of the *a*- and *b*-oriented crystals ammonia TPD was performed on the crystals with Si/Al = 125. As can be observed from Figure 3.2, the ratio of acid sites between the two different crystals are vastly similar. Making it reasonable to compare the result the two samples on a basis of the accessibility of the channels rather than a difference in acidity.

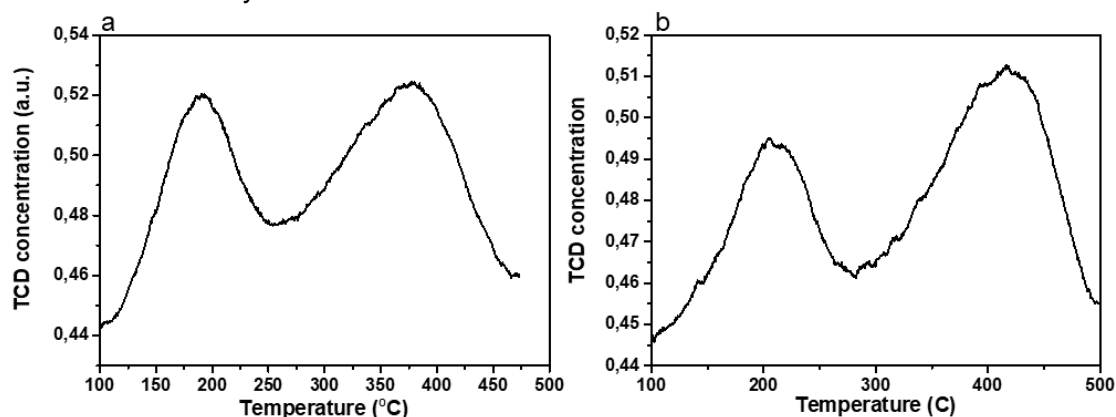


Figure 3.2 NH_3 -TPD profile of (a) *a*-oriented 125 and (b) *b*-oriented ZSM-5 crystals with Si/Al = 125

By converting the area below the graph to the quantity in mL NH_3 per gram of catalyst, the acid site density can be calculated by using the ideal gas law (3). With the assumption that a single ammonium molecule binds to a single acid site, the number of moles of ammonia desorbed per gram of catalysts directly corresponds to the amount of moles of acid sites per gram of sample.

$$PV = nRT \quad (3)$$

Table 3.2 Acid site density of *a*- and *b*-oriented ZSM-5 as calculated by NH_3 temperature programmed desorption

Si/Al ratio	a-ZSM-5 acid density	b-ZSM-5-125 acid density
125	$172 \mu\text{mol/g}$	$145 \mu\text{mol/g}$

The acidity as calculated from ammonia TPD is reasonably comparable, between *a*- and *b*-oriented crystals. Showing that the differences in their catalytic properties will largely be caused by the orientation in which they are grown and not their acidity, resulting in good model systems for the methanol-to-hydrocarbon synthesis.

3.2 Operando UV-Vis spectroscopic Studies of the Methanol-to-Hydrocarbons Process

The *a*- and *b*-oriented crystals with a Si/Al ratio of 125:1, as characterised in the previous paragraphs were employed in the industrial methanol-to-hydrocarbons reaction, while *operando* UV-Vis was measured with on-line GC. The spectra are plotted within the first few minutes, as those are dominated by the orientation of the crystals.

3.2.1 Deactivation behaviours and product distributions

a- and *b*-oriented zeolite ZSM-5 crystals were prepared with roughly identical sizes of approximately 2.0 μm with a Si/Al ratio of 125, according to the synthesis conditions. *a*-oriented zeolite ZSM-5 crystals have leaf-shaped plate-like shape with the sinusoidal channel dominating the surface, consistent with the morphology reported in the literature⁵⁵. *b*-oriented crystals exhibit a coffin-like shape, with straight channels primarily open to the surface⁵⁵. Samples of each catalyst exhibit discernible facets and a relatively monodisperse crystal size. According to the NH₃-TPD analysis, the catalysts show roughly similar acid site densities of approximately 155 $\mu\text{mol/g}$.

We first compare the deactivating rate of *a*- and *b*-oriented zeolite ZSM-5 crystals, where the difference in channel distribution have a marked influence on the deactivation behaviours. As shown in Figure 3.3, the deactivation of the *a*-oriented crystals is constant, while the deactivation of *b*-oriented ZSM-5 crystals happens in 3 stages. After a, relative to *a*-oriented crystals, slow deactivation rate for approximately 30 hours there is a steep drop in conversion observed, after which it follows a similar deactivating profile compared to *a*-oriented crystals.

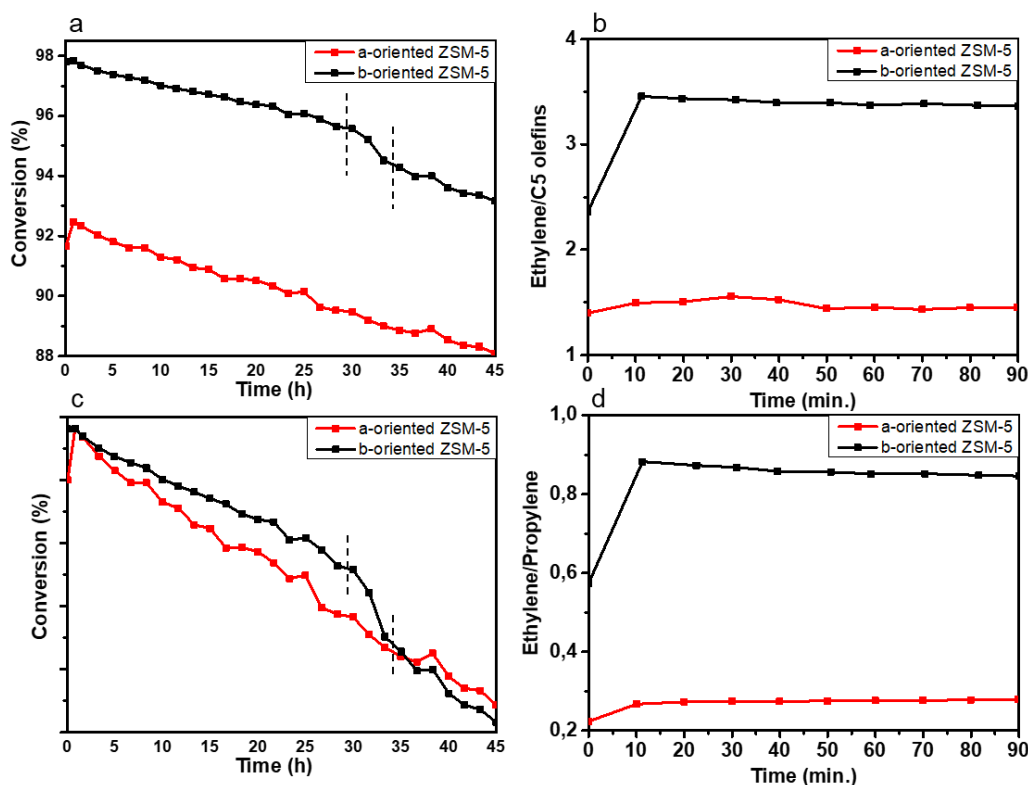


Figure 3.3 The conversion (a, c) of *a*- and *b*-oriented ZSM-5 in MTH synthesis at 350 °C with a WHSV of 5 h⁻¹, in c the graphs are shifted based on the data point with the highest conversion, to compare the deactivation slope. The (b) ethylene/C5 olefins and (d) ethylene/propylene are given, showing the relative propagation of the olefin and aromatic cycle and the ratio of the essential MTO products respectively.

Interestingly, the ratio between ethylene and 5C olefins (e.g. 2-methyl-2-butylene) is different throughout the entire reaction, with a higher ethylene/5C olefins ratio for *b*-oriented crystals. Ethylene/2MB ratio is often used as a descriptor for the propagation of the aromatic and olefin based cycles of the HCP mechanism⁴³. It is known that the aromatic cycle produces mainly ethylene and some propylene, while the olefin based cycle produces mainly propylene and higher olefins³⁹. Therefore the difference in the Ethylene/5C olefins ratio, shows the enhanced propagation of the aromatic cycle within the *b*-oriented channels, whereas *a*-oriented channels show a more pronounced propagation of the olefin based cycle.

3.2.2. Evolution of hydrocarbons studied with operando UV-vis spectroscopy

To explain the differences in life-time and product distribution, *operando* UV-Vis diffuse reflectance spectroscopy (UV-Vis DRS) was employed, as it is an insightful technique for the detection of HCP and coke species formed in zeolites during the MTH process. In the first minutes, small aromatics (<300 nm) are promoted within the *a*-oriented channels (highly accessible for *a*-oriented crystals) and larger HCP species (300-400 nm) are formed earlier in the *b*-oriented channels (highly accessible for *b*-oriented crystals). This difference vanishes after longer reaction times, as internal diffusion reaches throughout the entire crystal, resulting in similarly looking UV-Vis absorption spectra for both orientations.

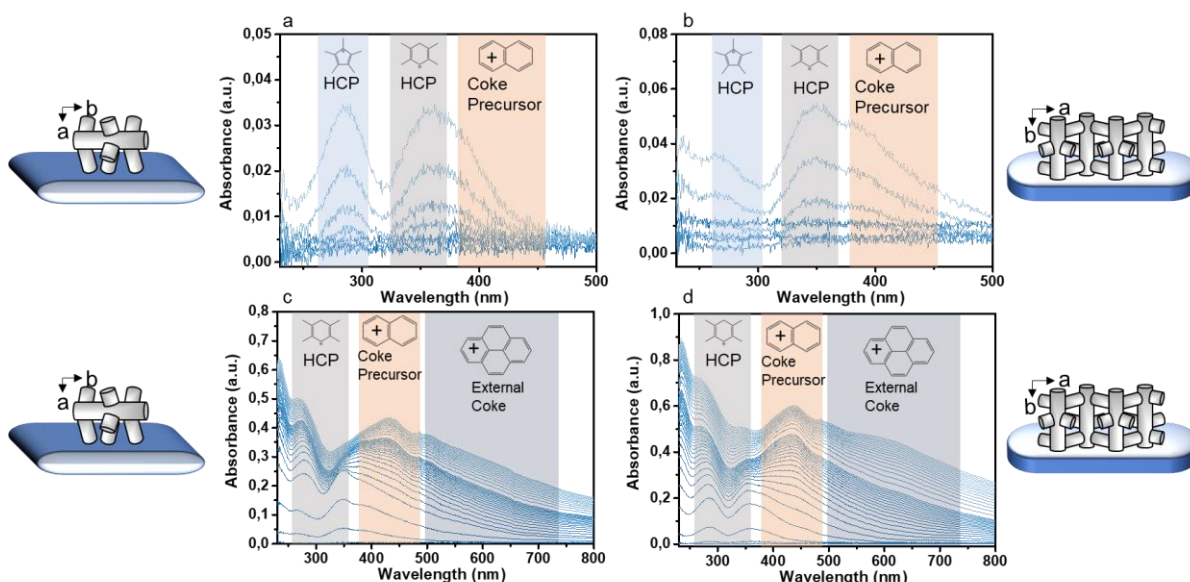


Figure 3.4 Operando UV-vis of (a) *a*- and (b) *b*-oriented ZSM-5 Crystals in their first 1.5 minutes of MTH reaction at 350 °C with a WHSV of 5 h⁻¹.

3.2.3. Study of retained hydrocarbons in the first reaction stage

To study trapped organics inside the oriented crystals, a setup with a Linkham cell was used. The crystals were placed on the stage, heated to 350 °C for 1 hour before reaction. The reactions was run for either 3 or 10 minutes, with a 15 mL/min N₂ flow through a saturator containing methanol, after which the cell was cooled down and the reacted crystals were recovered. After reaction the trapped hydrocarbons were studied ex-situ, by UV-Vis spectroscopy, taken with an UV-Vis probe, wherein fresh oriented crystals were used as a reference. After reference, the samples were placed under the probe, showing the hydrocarbon species present inside the zeolite crystals after 3 and 10 minutes of reaction.

Clearly, after 3 minutes the larger hydrocarbon pool species are present in *b*-oriented crystals, that have a higher accessibility for *b*-oriented channels. After 10 minutes the hydrocarbon pool species are vastly similar within both crystals, although a higher absorption is observed for *a*-oriented ZSM-5 for either coke precursors or external coke species.

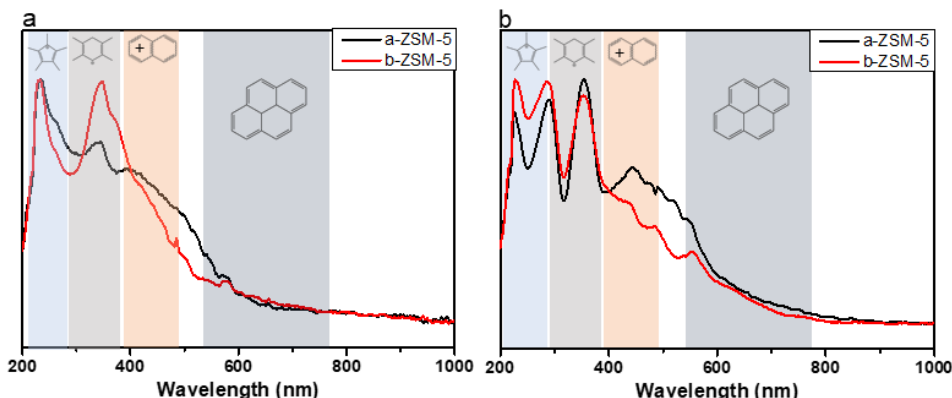


Figure 3.5 Ex-situ UV-vis of *a*- and *b*-oriented ZSM-5 crystals after (a) 3 and after (b) 10 minutes respectively.

To identify the actual trapped carbons within these *a*- and *b*-oriented channels after 3 minutes of reaction the crystals were dissolved in 45% HF, after which the organics were extracted by CH_2Cl_2 . This organic layer was studied using GC-MS (Figure 3.5). A coupled ^{13}C NMR measurement was taken as well, as a non-destructive method to investigate trapped aromatic species. Unfortunately no significant signal was obtained during the ^{13}C NMR experiments. Probably, because of the relatively low carbon content in the sample, after such a short reaction time.

In the GC-MS samples a mostly similar chromatogram is observed, however, there are some very telling differences. The most important peaks are highlighted in Figure 3.5, showing that the methylated HCP aromatic is more pronounced in the *a*-oriented channels, promoting small aromatics ($m/z = 135$), whereas *b*-oriented channels already show large conjugated coke species ($m/z = 191$) (the MS spectra of the assigned species in the GC-MS measurement are shown in the supporting information in Figure S1). This is another confirmation that the *a*-oriented channels enhance the formation of small HCP species and that the *b*-oriented channels promote the formation of internal coke species. It has to be noticed, however, that while the conjugated coke species are more pronounced in the *b*-oriented crystals, they are present in the *a*-oriented ZSM-5 crystals as well. This can be explained due to the contribution of hydrocarbon species not being exclusively from a single channel. The accessibility to a certain channel within those first few minutes is the major reason for the difference in intensity, while contributions of both channels can still be observed in either sample. Many peaks are not assigned, as they do not belong to a carbon species, but are leftovers of the zeolite framework.

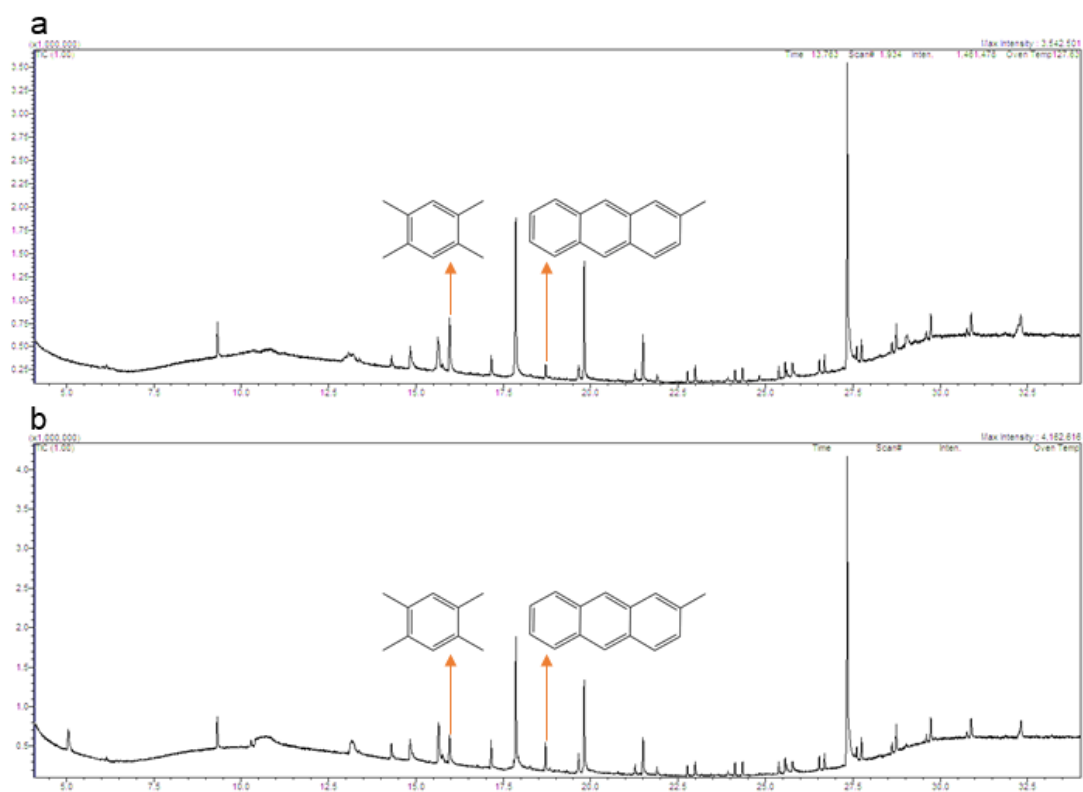


Figure 3.6 GC results of the products extracted from (a) *a*-oriented ZSM-5 and (b) *b*-oriented ZSM-5 crystals after 3 minutes of MTH synthesis.

4. Reaction Behaviours studied on Oriented Thin-Films

To extend the insights obtained from the previous chapter on oriented crystals, oriented ZSM-5 thin-films were synthesised and studied as model systems in thiophene and 4-methoxystyrene oligomerisation reactions, as well as the methanol and ethanol-to-hydrocarbons synthesis.

4.1 Fabrication of Oriented Zeolite Thin-Films

4.1.1 Synthesis of oriented zeolite seed crystals

After the synthesis of the *a*- and *b*-oriented purely siliceous MFI (silicalite-1), the seed crystals were checked for their orientation, size and the presence of intergrowths. As seen in Figure 4.1 the *a*- and *b*-oriented seed crystals, while having some intergrowths, are mostly uniform in orientation as well as in size (~2 μm). So, they are suitable for the formation of an MFI monolayer.

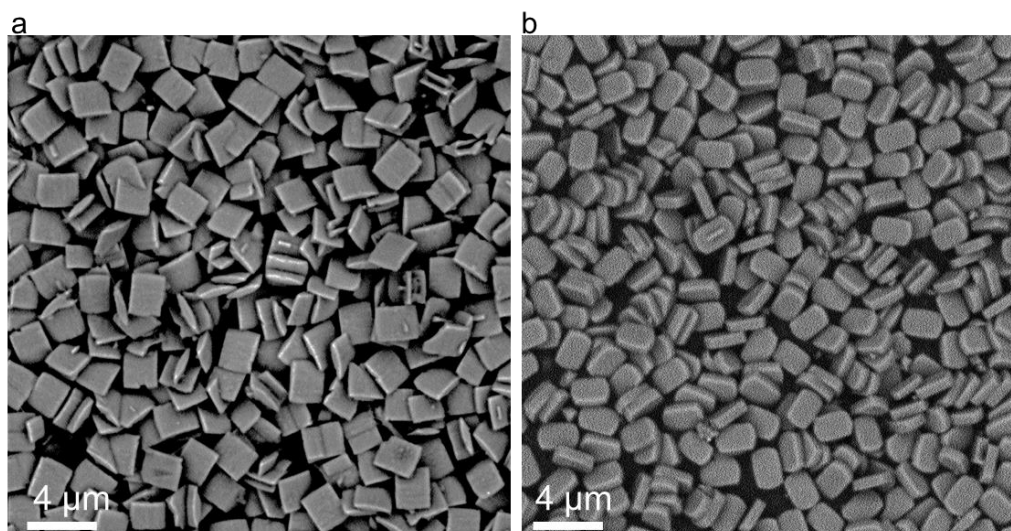


Figure 4.1 SEM image of purely siliceous (a) *a*- and (b) *b*-oriented MFI crystals, used as seed crystals for monolayers synthesis.

4.1.2 Attachment of oriented zeolite monolayers

Different procedures have been used to synthesise uniformly *a*-oriented monolayers. These methods consist of spin-coating and chemical functionalisation of the substrate followed by refluxing, sonification or manual assembly to adhere the *a*-oriented seed crystals. For spin-coating, a polymer (glue, e.g. PEI) is applied on the substrate, after which the seeds were attached by manual assembly⁵⁵. Another applied technique is chemical deposition, in which the substrate was refluxed in an organic binder molecule (e.g. 3CP-TMS) followed by either sonification⁵⁶ or refluxing of the seed crystals and the substrate in toluene⁵⁷. It is also possible to first apply a silica layer on a substrate by dip-coating, after which the surface is functionalised and the crystals were applied as described before⁵⁸. An overview of all techniques described here is given in Table 4.1.

Table 4.1 *a*-oriented monolayer synthesis techniques used in literature.

Method of substrate treatment	Attachment of seed crystals	Reference
Spin coating (PEI in ethanol)	Manual assembly	Tung et al. ⁵⁵
Chemical deposition with 3CP-TMS	Sonification	Choi et al. ^{56,12}
Chemical deposition with 3-amino-propylsilyl	Refluxing of crystals in Chemical deposition with 3-amino-propylsilyl followed by refluxing in toluene	Choi et al. ⁵⁷
Dip-coating in silica layer, followed by chemical deposition	Both reflux and sonification techniques were used	Kim et al. ⁵⁸
-	Sonification of seeds in toluene on bare α -alumina disks	Kim et al. ⁵⁸

There were 2 methods used here: spin-coating and dip coating, after which manual assembly was applied to attach the seed crystals. Generally, polyethylenimine (PEI) in ethanol solution was made, in which the concentration was varied from 0.3 to 1 wt.%. Besides that, epoxy and polyethylene glycol (PEO) were tried as a glue, but they were ineffective and were discarded early on.

For the spin-coating method the spin-coating speed, the PEI concentration, as well as the amount of polymer solution added were varied. The quality of the monolayer was examined for 2 properties, which is both the coverage (amount of area covered by a monolayer, visible by eye) and the packing (the amount of empty space and the orientation of the crystals, visible by SEM). The spin-coating speed at low rpm, resulted in a poor coverage of *a*-oriented MFI seeds after manual assembly. Presumably, because the polymer did not disperse well over the quartz plate, leaving entire spaces open, with no 'glue' present to attach the seeds. It has also been tried to repeat the spin-coating after the first manual assembly, however, this resulted into even more out of plane crystals and did not improve the monolayer quality at all. At higher speeds and amount, speed ≥ 2500 rpm and amount ≥ 200 μ L, there was polymer present all over the quartz plate, resulting in fully covered quartz plates. However, when those synthesised monolayers were examined with SEM (Figure 4.2), the packing of the seed crystals was poor. Showing plenty of empty space, combined with misdirected, out of plane, crystals at different spots. Possibly, this was caused by an abundance of polymer, limiting the mobility of the seed crystals, sticking only to the place where they were attached. In addition to that the crystals that were applied out of plane did not disperse and remained misdirected. Unfortunately, while this method does

show a fully covered quartz plate by eye, no acceptable middle ground has been found, as shown in Figure 4.2. It has to be mentioned that in contrast to the spin-coating method reported by Pham et al.⁵⁵ no PDMS was applied on the substrate before spin-coating with PEI. A method that provides both a good coverage over the entire quartz plate, as well as a good micrometre lever packing is desired here.

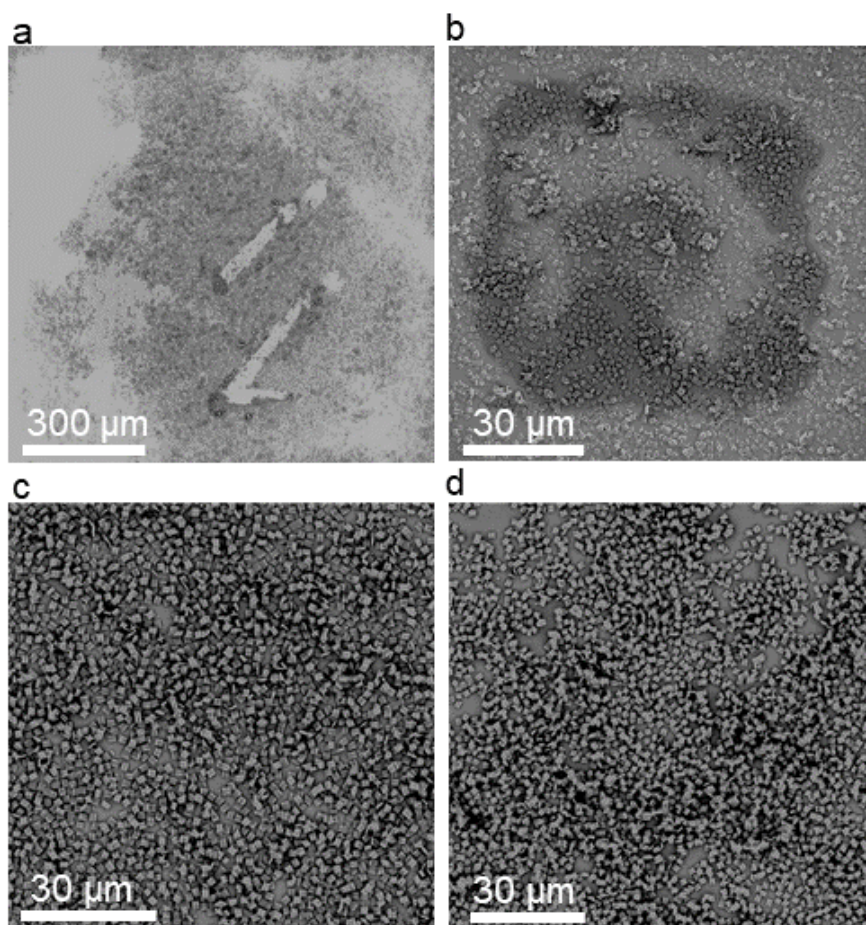


Figure 4.2 (a) Monolayers containing plenty of empty space after spin coating, (b) monolayer spin-coated with epoxy with a poor packing, (c) high amount of out of plane crystals after spin coating, (d) high amount of out of plane crystals after double spin-coating.

Therefore, a dip-coating method was tried, wherein the quartz plate was submerged within the PEI in ethanol solution. The time submerged was varied, as well as the PEI concentration of the solution. In these experiments similar trends were observed, compared to spin-coating. At low PEI concentration (0.3 wt.%) poor coverage of the polymer on the quartz plate was observed, which resulted in poorly covered monolayers. On the other hand, at higher PEI concentration (1 wt.%), full coverage was observed, but it was not well packed. For dip-coating, however, a decent balance was found at 0.5 wt.% PEI concentration, showing reasonable coverage, combined with a reasonable packing. Further optimisation resulted in the PEI concentration of 0.425 wt.%, while the substrate was submerged for 2 minutes. The attempted parameters for spin- and dip-coating are summarised in table 4.2.

Table 4.2 Attempted parameters for coating of polymer (PEI) on top of a glass/quartz substrate.

Method		PEI concentration (wt.%), amount (μl)	Time (s)	Result
	rpm			
Spin coating	1500	0.5, 200	15	Poor coverage
	2500	0.3, 200	15	Poor coverage
	2500	0.5, 200	15	Fully covered on the quartz plate, not densely packed under SEM.
	2500	1, 200	15	Fully covered on the quartz plate, not densely packed under SEM.
	3500	0.5, 200	15	Fully covered on the quartz plate, not densely packed under SEM.
Dip coating		0.3	120	Poor coverage
		0.425	120	Best result so far
		0.5	120	Reasonable result
		0.75	60	Fully covered on the quartz plate, not densely packed under SEM.
		1	60	Fully covered on the quartz plate, not densely packed under SEM.

As described before, the dip-coating method was the most successful in providing both good packing as well as orientation. This resulted, in general, in good monolayers as shown in Figure 4.3. Although the *a*-oriented monolayers were not always as homogeneously covered over the quartz plate and many attempts were still needed to get an excellent result.

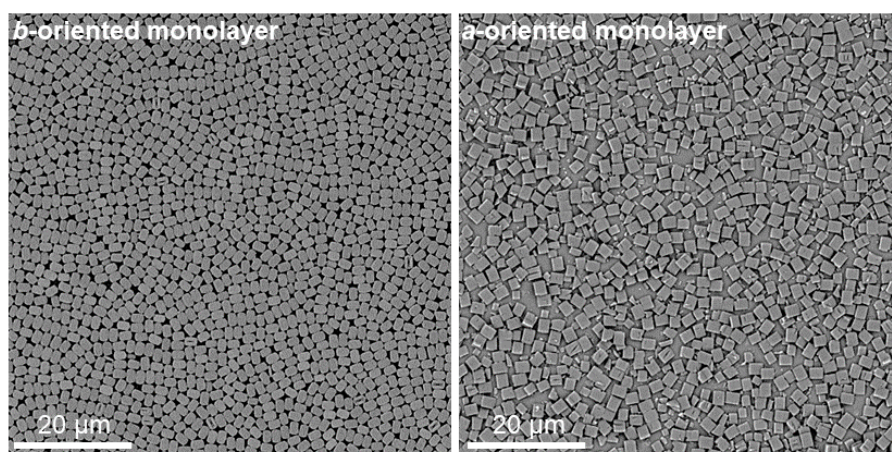


Figure 4.3 SEM images of *a*- and *b*-oriented monolayers MFI seed crystals on a (PEI coated) quartz substrate, with the accordingly measured XRD.

For *b*-oriented monolayers the crystals were applied directly on the surface of the cleaned quartz plate by a manual assembly method, described in earlier work by D. Fu⁵⁹. Due to the electrostatic interactions of the crystals and the surface, these hexagonal crystals can be applied after careful rubbing, resulting in well covered monolayers over the entire quartz plate.

4.1.3 Growth of continuous zeolite thin-films

From the oriented monolayers studied in the previous paragraph, thin-films were grown in a secondary growth medium (SGM) with Si/Al = 45 and 125. These were then studied with SEM and XRD to determine their orientation and quality, which refers to either the coverage, intergrowth and presence of amorphous silica. In Figure 4.4, the *a*-oriented thin-films with different Si/Al ratios are shown. Here, it can be observed that for SGMs with Si/Al = 125 and 45 highly *a*- and *b*-oriented ZSM-5 films were obtained, although the *a*-oriented thin-films are not completely covered and show a small amount of out of plane crystals.

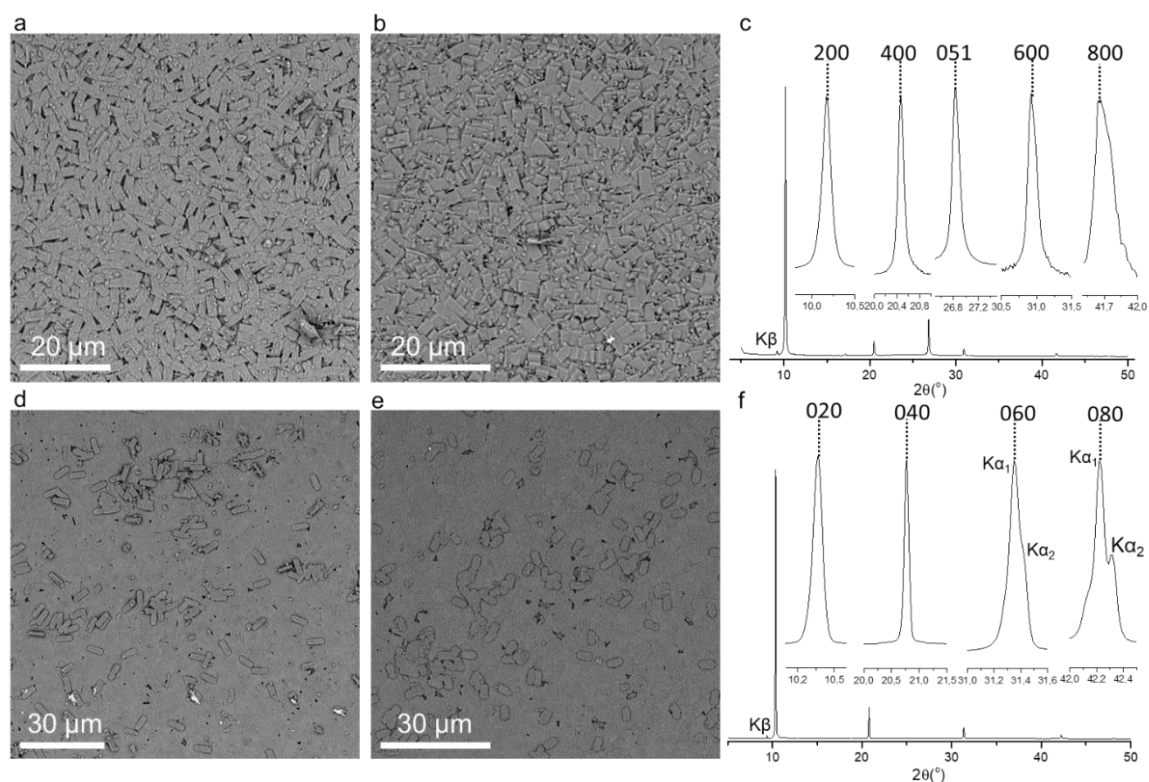


Figure 4.4 SEM images of (a, b) *a*- and (d, e) *b*-oriented thin-films after secondary growth in a SGM with Si/Al ratios of (a, d) 125 and (b, e) 45 with a representative XRD spectrum of (c) *a*-oriented ZSM-5 and (f) *b*-oriented ZSM-5 respectively.

However, the *a*-oriented thin-films, as produced here, can be used for MTH reaction, wherein the channels perpendicular to the orientation are probed. The *b*-oriented thin-films, however, are very continuous and well grown over the entire thin-film. Besides that, the position of the Brønsted acid sites are determined by the aluminium siting within the framework. By conducting the secondary growth, with a non-SDA route, containing sodium ions, the acid sites are not exclusively present within the channel intersections, but more widely dispersed, predominantly throughout both channels, but also present in the intersection⁶⁰. This provides good model systems, with uniformly oriented channels and uniformly dispersed acid sites. In the X-ray diffractogram can be observed that these thin-films are solely crystalline ZSM-5 and oriented correctly^{4,12,61}, showing only a couple of ZSM-5 peaks, as the thin-film is oriented and only certain planes can show constructive interference.

4.2 Oligomerisation Reactions

Insight into the difference in the contribution of channel specific behaviour to product formation in simplified reactions was obtained. Firstly, 4-methoxystyrene oligomerisation products consist of two well defined structures, giving information about the channel specific properties. These are the dimeric and trimeric carbocation, which is present in both channels and just in *b*-oriented channels respectively (Table 4.3). The presence of these bulkier species inside the straight channels is also observed in the as-prepared oriented thin-films (Figure 4.5).

Table 4.3 Assignment of the UV-Vis absorption peaks for 4-methoxystyrene oligomerisation.

Wavelength (nm)	Assignment	Channel	Reference
630	Trimeric carbocation	<i>b</i> -oriented	Ristanovic et al. 25
580	Dimeric carbocation	Both	Ristanovic et al. 25
340	Protonated monomer	Both	Cozens et al. ⁶²

This same trend is observed in the thiophene oligomerisation reaction. In Figure 4.5 (c, d), it is shown that larger oligomers are formed in the *b*-oriented channel. The molecules up to 553 nm are quite well assigned (Table 4.4), as either a thiophene oligomer formed from direct oligomerisation or as a result of the ring opening mechanism. Due to the relatively large amount of absorbance at larger wavelengths than 553 nm it can be stated that even larger oligomers form inside the straight channels. As larger oligomers, due to an increased delocalised π system, are more stabilised, resulting in a red-shift in the UV-Vis absorption wavelength³⁰.

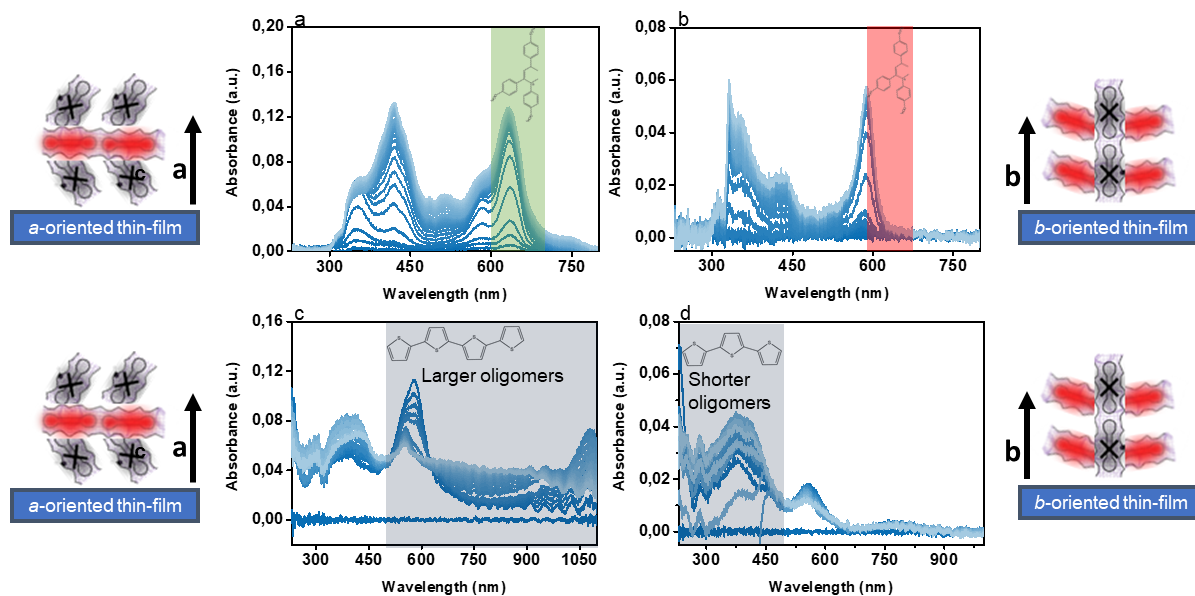


Figure 4.5 UV-Vis spectra of (a, b) 4-methoxystyrene and (c, d) thiophene oligomerisation on oriented thin-films, showing the (a) presence of the trimeric carbocation in green and its (b) absence in red.

Table 4.4 Assignment of the UV-Vis absorption peaks for thiophene oligomerisation.

Wavelength (nm)	Assignment	Reference
298	Monomer+	D. Valencia et al. ⁶³
340	Dimer+	D. Valencia et al. ⁶³
404	Trimer+	D. Valencia et al. ⁶³
440	Ring opening product+	G. Whiting et al. ²⁹
553	Tetramer+	D. Valencia et al. ⁶³
579	Larger oligomer	-

Therefore, it can be concluded from both of these probe reactions that the *b*-oriented channels promote the formation of extended molecules, whereas the formation of larger molecules is suppressed in the *a*-oriented channels. This is found throughout the multitude of different reactions performed and can be used in comparison to how the hydrocarbon pool molecules in the industrial methanol- and ethanol-to-hydrocarbons synthesis.

To validate these differences on the ex-situ sample, an UV-Vis probe spectrum was taken (Figure 4.6b) of a 4-methoxystyrene sample, proving the consistency of the existence of the molecules inside the assigned channel as described above. Another validation of the methodology, showing that the difference in the spectrum are based on the channel and not on other differences between the thin-films, is a tilt series of an *a*-oriented thin-film after 4-methoxystyrene oligomerisation with CFM.

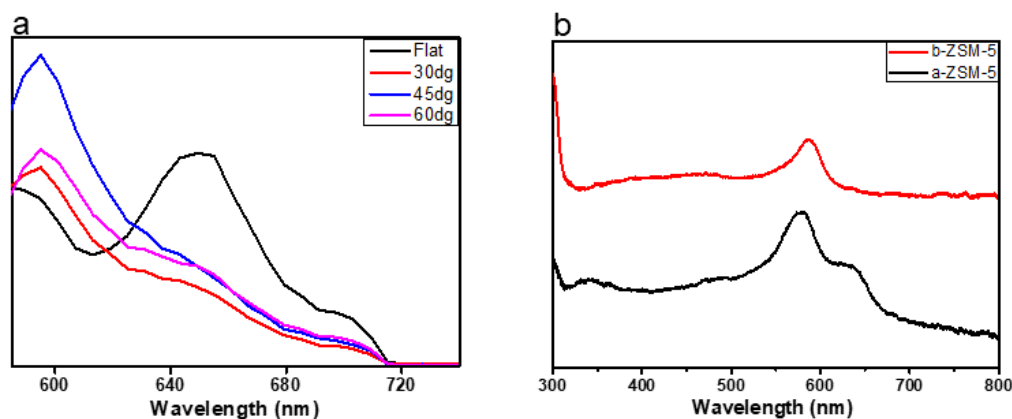


Figure 4.6 (a) Tilt series of *a*-oriented zeolite ZSM-5 thin-film with Si/Al = 125 after 4-methoxystyrene oligomerisation. (b) Ex-situ UV-Vis of *b*-oriented ZSM-5 and *a*-oriented ZSM-5 thin-films after 4-methoxystyrene oligomerisation.

As mentioned before, the orientation of channels that can be probed are those that are perpendicular to the orientation of the thin-films (chapter 1.2). This constitutes that the peak that is only present in the *a*-oriented thin-film, will largely disappear when the sample is tilted under a certain angle. This is done by applying the ex-situ sample to a stage with 3 facets. Cut at angles of 30°, 45° and 60°, to which sticky tape is present on which the sample can be applied. This disappearance of the 650 nm peak is exactly what can be observed in Figure 4.6, for the emission data, the peak at 595 nm is assigned to the dimeric carbocation, whereas the peak at 650 nm is assigned to the trimeric carbocation. That the signal assigned to the trimeric carbocation disappears with the tilt series, proves that the trimeric carbocation is not just a feature of the *a*-oriented thin-film sample, but is exclusively present within the *b*-oriented channel.

4.3 Alcohol-to-Hydrocarbons Processes on Zeolite ZSM-5 Thin-Films

The observations from the probe reactions show the difference in the shape selectivity inside the different channels of the zeolite ZSM-5 framework. Showing that the formation of bulkier molecules is promoted inside *b*-oriented channels, and suppressed in the *a*-oriented channels. Using UV-Vis diffuse reflectance spectroscopy, the same methodology was further applied for the industrial MTH reaction.

4.3.1 Operando UV-Vis on oriented ZSM-5 thin-films

It is known that the absorption by compounds aligned within a channel, does not occur when the dipole moment of the molecule is perpendicular to the polarisation of light⁵¹. This provides the ability to decouple the two different MFI channels, as shown alongside the UV-Vis spectra (Figure 4.7). The evolution of protonated HCP and small coke species (e.g. naphthalene) inside the *a*-oriented channels can therefore be monitored in *b*-oriented thin-films and vice versa. It has been generally acknowledged that methylbenzenium ions (up to 4 methyl groups) with absorption at 350 nm are the active species for MTH reactions in ZSM-5 catalysts³⁸. In Figure 4.7, a much higher intensity ratio of naphthalene carbocations (420 nm) to methylbenzenes (350 nm) was observed inside *b*-oriented channels and their accumulation may lead to pore blockage. Moreover, external coke species (four/ five-ring at 550-635 nm and poly-condensed aromatics > 675 nm), were more pronounced on the surface of *a*-oriented thin-films, illustrated by a much higher intensity ratio of external cokes to HCP species (Figure 4.7). A complete summary of the assigned UV-Vis active species is given in Table 4.5

Table 4.5 Assignment of the UV-Vis absorption peaks in methanol-to-hydrocarbons reactions.

Wavelength (nm)	Assignment	Reference
260	Neutral methylbenzenes	Wulfers et al. ⁶⁴
295	Cyclopentadienium ions	Wulfers et al. ⁶⁴
350	(4-5) Methylbenzenium	Wulfers et al. ⁶⁴
410	Two- three-ring aromatics	D. Mores et al.
>550 nm	Larger aromatics species/cokes	E. C. Nordvang et al. ³⁹

To generalise these findings, ethanol-to-hydrocarbons was also studied with the same approach. Analogues to MTH, a higher external surface to smaller coke species ratio was observed on *a*-oriented thin-films. Also, the relative ratio of HCP to small coke species is higher for *a*-oriented channels, showing the suppression of small coke species inside the sinusoidal channels. Interestingly, for both orientations a higher external to internal coke ratio was observed in comparison to MTH, as shown by a higher ratio of internal (420 nm) to external (> 550 nm) cokes (Figure 4.7).

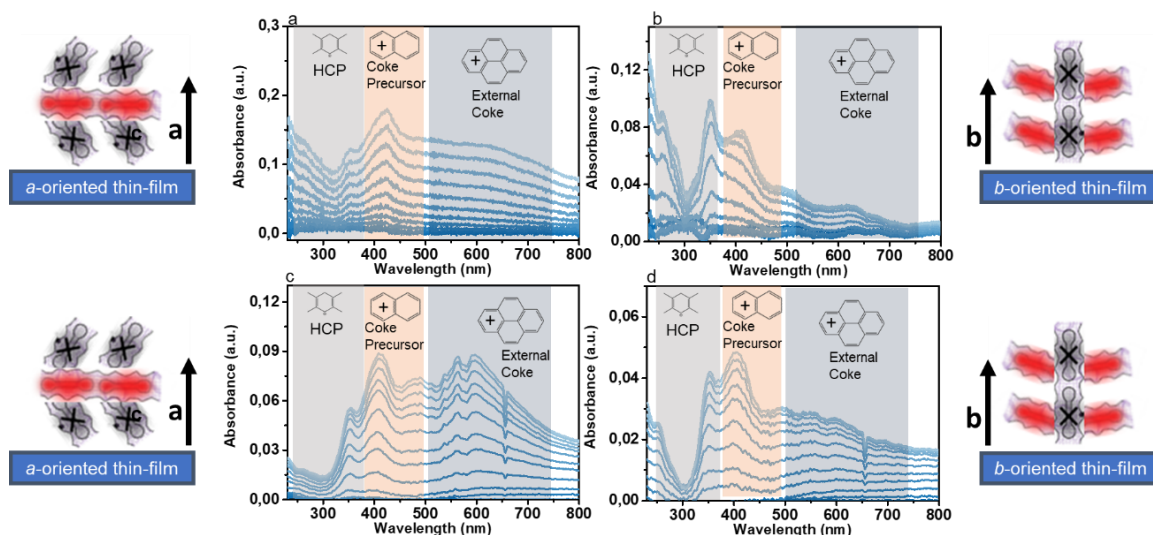


Figure 4.7 (a, b) Methanol-to-hydrocarbons and (c, d) ethanol-to-hydrocarbons on oriented thin-films during the first 3 minutes of reaction with the probed channel being depicted on the left and the assigned molecules depicted inside the spectra, which are active HCP species, coke precursors and external coke.

Meanwhile with on-line MS, as shown in Figure 4.8a, toluene was observed in the effluent of *a*-oriented thin-films. *b*-oriented thin-films on the other hand did not show toluene in a significant manner at all. Therefore we speculate that, due to their tortuous structure, the formation of small coke species is suppressed within the *a*-oriented channel, allowing toluene to diffuse out and conjugate to large coke species on the external surface, as shown in Figure 4.8b. The *b*-oriented channel, on the other hand, will get blocked by the formation of small coke species. For ETH, however, no toluene was found in the effluent of either oriented thin-film. The effluent of toluene over the entire reaction of both MTH and ETH is shown in the supporting information in Figure s5.

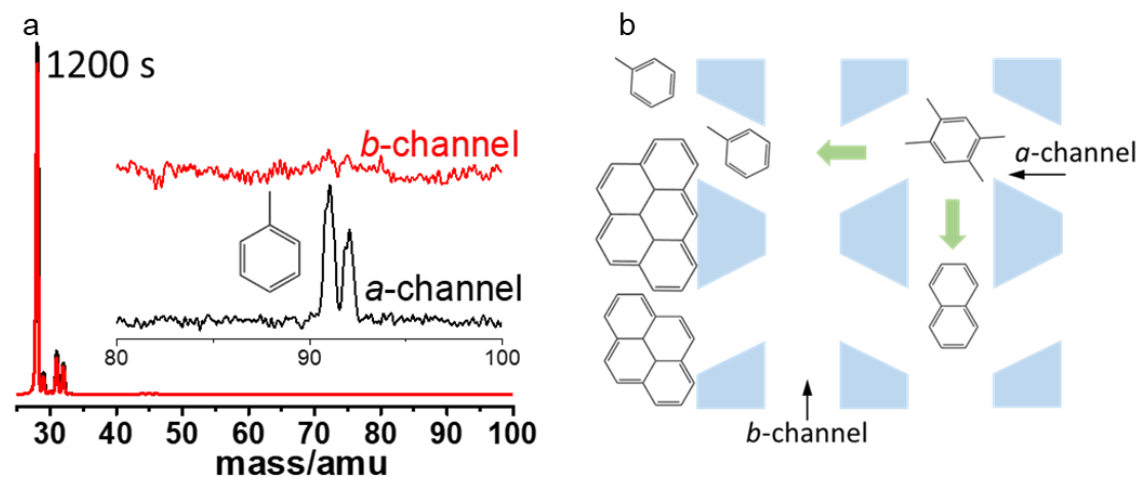


Figure 4.8 (a) MS spectrum after 1200 seconds showing toluene present in the effluent of *a*-oriented thin-films, but not in the effluent of *b*-oriented channels. (b) The proposed model based on the presence of toluene in the effluent of *a*- and absence from *b*-thin films.

It has been reported for ETH on SAPO-34, that external coke species formed first⁶⁵. The first detectable coke species for ETH were external, with the small coke species following up. However, for MTH the internal coke species dominate at the start of the reaction, with a gradual build-up of coke species over time. This is in accordance with the claim that external coke species form first in the ETH reaction, regardless of the facets. Therefore, we speculate that the formation of external coke species consumed the aromatics that could effluent out from the *a*-oriented channel, attributed to the absence of aromatics in the

MS spectra. Collectively, these results suggest that deactivation in ETH starts from the surface of the thin-films, followed by pore blockage.

4.3.2 Ex-situ assessment of the location of the coke species

In addition to the information obtained by UV-Vis, CFM was applied to visualise the large external coke species by using a 561 nm excitation laser. The emission of external coke molecules, similar to the one shown in the red box (Figure 4.9), can be observed⁶⁶. In Figure 4.9, it is shown that the surface of the *a*-oriented thin-films has a much stronger emission, compared to the *b*-oriented thin-films. Similar trends were observed for oriented zeolite thin-films with a Si/Al ratio of 45. The reconstructed 3D image is obtained by applying the thin-films to a stage, and then shifting its focus point by adjusting the height of the stage, showing how the external coke is positioned on the zeolite thin-films..

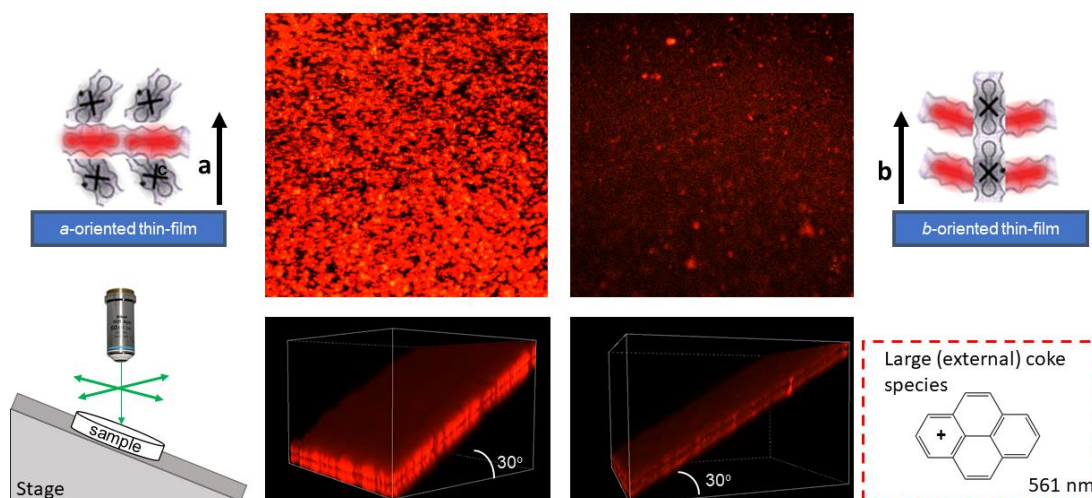


Figure 4.9 Confocal fluorescence microscopy image of oriented thin-films with Si/Al = 125 excited by a 561 nm laser (top), as a flat substrate and with a 30° tilt on a stage (bottom). In the red box an example of the kind of coke species probed by the 561 nm laser is given.

For the analysis of the trapped species within the oriented thin-films after reaction the probe was used ex-situ. Used samples, were applied on a stage at a certain tilt, similar to CFM, and the probe was used to take an absorbance spectrum (Figure 4.10), with a fresh thin-film as reference. It can be observed that inside the *b*-oriented channel (flat *a*-oriented thin film) the absorbance is exclusively in the higher wavelength regions, showing both the external coke formation that is on the surface of the *a*-oriented thin-films (>550 nm), as well as the smaller coke species trapped inside the straight channel (>410 nm). The external coke formation is more pronounced on the surface of the (Figure 4.10a, c) flat *a*-oriented thin-films compared to the (Figure 4.10b, d) *b*-oriented surface, only showing a relatively small amount of absorption at wavelengths larger than 500 nm³². When tilted, however, it shows the contribution of the species in the *a*-oriented channel, which consists of smaller, possibly HCP active, aromatic species between 300-400 nm (Table 4.5). When analysing the (Figure 4.10b, d) *a*-oriented channel ex-situ, it shows strong absorbance of HCP aromatics, which indicates that these species are truly present in the channel and do not form because of other sample difference. Further confirming the proposed mechanism as shown in Figure 4.8, as well as the enhanced formation of larger coke precursors inside the straight *b*-oriented channels and smaller HCP aromatics inside the sinusoidal *a*-oriented channels.

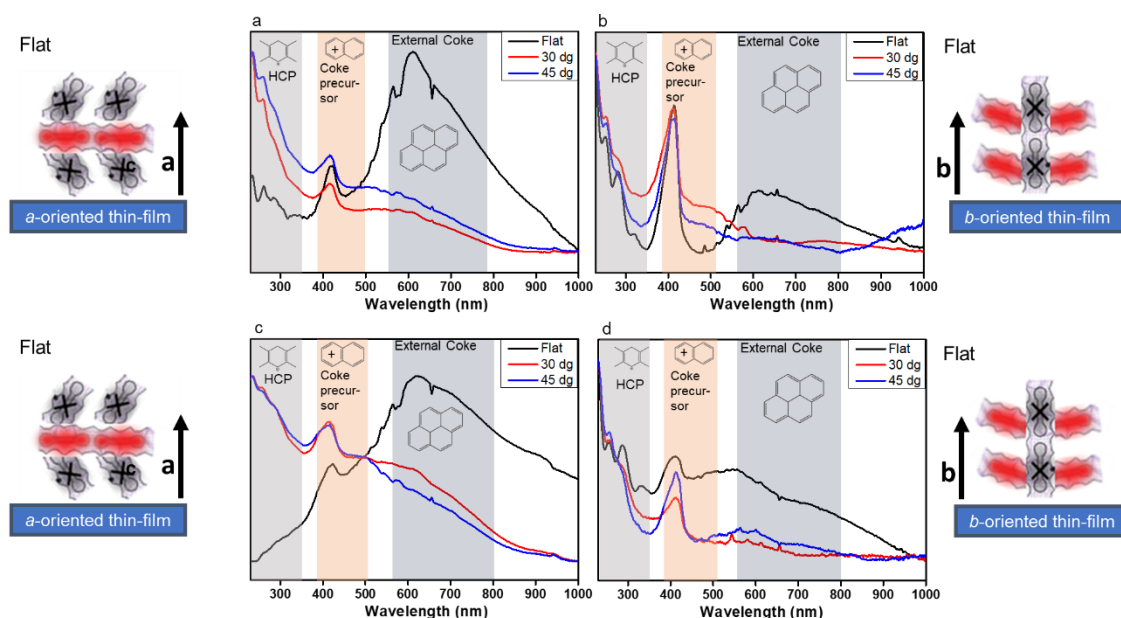


Figure 4.10 Ex-situ comparison of oriented thin-films as flat substrates compared to a 30- and 45-degree angle. The images next to the spectra, show the orientation of the thin-film when the substrate is flat.

5. Conclusions & Outlook

5.1 Conclusions

In this thesis, oriented zeolite ZSM-5 crystals and thin-films were synthesised and applied as reaction platforms to study the reaction behaviours in single zeolite channel orientations using a spectroscopic approach.

In the first part, the deactivation behaviours and product distributions during the MTH process on oriented crystals were investigated. The crystal morphologies and crystallinities were measured with SEM and XRD, respectively. The evolution of hydrocarbons in the crystals and product distributions were monitored using *operando* UV-Vis coupled with GC. The product distribution showed that crystals with a higher accessibility to *a*-channels have a more pronounced olefin based cycle, relative to the *b*-oriented crystals. Multiple deactivation stages were observed in *b*-oriented ZSM-5 crystals, while *a*-oriented crystals showed a constant deactivating rate during reaction. To study this deactivation, the formed species within the crystals were monitored with *operando* UV-Vis, showing the earlier formation of more conjugated species in *b*-channels. The retained hydrocarbons, as analysed by GC-MS, also show small coke species within the higher accessible *b*-channels.

Secondly, due to the uniform crystallographic orientations of oriented zeolite thin-films, evolution of hydrocarbons and products in each channel orientations can be exclusively followed with *operando/in-situ* UV-Vis spectroscopy coupled with mass spectrometry. The results from the in-situ oligomerisation reactions demonstrate that extended hydrocarbons are preferentially formed in *b*-oriented channels (straight), while they were suppressed in the *a*-oriented channels (sinusoidal). For the MTH process it was found that, similar to oriented crystals, more conjugated species were formed inside the *b*-oriented channels. Interestingly, toluene was observed in the effluent from the *a*-oriented channels during MTH, as measured by MS. This, combined with the more pronounced external coke on the surface of the *a*-oriented thin-films, has led us to speculate that the *b*-oriented channels gets blocked by small, internal coke species, while the tortuous *a*-oriented channels suppress their formation. These small aromatic species, in *a*-oriented channels, can therefore diffuse to the external surface, followed by conjugation forming large external coke species. The gained insight on the channel specific reaction behaviours, show that the deactivation of the crystals is largely dominated by external coke, as highly *a*-oriented crystals deactivated faster. At a later stage, both internal and external coke contribute in a major way and the deactivation slope becomes comparable.

To summarise, using both oriented crystals and thin-films, a panoramic picture has been built for the reaction behaviours in single zeolite channel orientations. We believe that the knowledge obtained from this thesis could benefit the chemical industry in designing new zeolite materials for targeted products, and that the research approach innovated in this thesis opens a new way for studying structure-performance relationships of zeolite catalysts during chemical reactions at a single zeolite channel orientation level.

5.2 Outlook

Improvements to the *a*-oriented thin-films could be achieved, by improving either the monolayer quality or the secondary growth method. Especially the density of crystals in monolayers dictates the thin-film quality. Other methods, including chemical attachment, could also be tried. These improved thin-films would operate as superior model systems, and in an ideal case, might even be usable as molecule separation membranes.

Pyridine-IR could be applied on the oriented crystals, to give additional information besides NH_3 -TPD on the acid site nature, such as the Lewis to Brønsted acid site ratio. To study the trapped species inside the zeolite channels with ^{13}C NMR, ^{13}C labelled methanol could be used for MTH on oriented crystals after short time reaction, that will lead to the entrapment of hydrocarbons primarily in corresponding channels. However, the crystals with a Si/Al ratio of 125 did not show enough NMR signal after 3 minutes of reaction. Therefore, oriented crystals with lower Si/Al ratio, e.g. 20, can be synthesised for the NMR measurement.

Confocal fluorescence microscopy might be employed during the MTH reaction. This will provide additional insight into the reactivity and kinetics of the two distinct channels in the ZSM-5 MFI framework, as well as the build-up of external cokes. Additionally, UV-Raman could be used to analyse the formation of external coked on the oriented thin-films, as it gives insight into the aromaticity (graphene like structure) of the formed coke. This could both be performed ex-situ as well as, preferably, in-situ.

Acknowledgements

After doing research at ICC for over a year, my project has come to an end. First, I would like to thank my daily supervisor Donglong Fu, who helped me through all the experiments, writing and presentations. He was a great supervisor, who taught me a great deal. I would also like to thank Bert M. Weckhuysen for being my first examiner and Florian Meirer for being my second supervisor.

I also would like to thank everyone who helped with mastering an analytical technique, who are Dennie Wezendonk and Marjan Versluijs-Helder for X-ray diffraction, Hans Meeldijk for SEM, Sophie van Vreeswijk and Ramon Oort for the *operando* MTH setup, Suzanne Verkleij for the trans-alkylation setup, Robert Geitner and Anne-Eva Nieuwelink for Raman and Beatrice Luna Murillo for pyridine-IR.

In addition to that, I would like to thank Alessandra Lucini Paioni for measuring ^{13}C NMR for us and Ad van Eerden for performing the HF extraction for me, as well as fruitful discussion, and Pascal Wijten for performing GC-MS. I would like to thank Gareth Whiting for insightful discussion on the interpretation of the probe reactions.

Besides that, I would like to acknowledge Kiki Schuurman and Jeroen Vonk for the enjoyable moments on the lab, when they were Bachelor's students under the supervision of Donglong (and sometimes myself). Jeroen Vonk's work, on which I partly continued, also helped a great deal by understanding the reaction behaviour within the oriented crystals.

Finally, I would like to thank all the master's and bachelor's students at ICC, especially the people sitting closest to my desk, who are: Thimo Jacobs, Jim de Ruijter and Jeroen Dubbeld. As well as Kristiaan Helfferich, Oscar Brandt-Corstius and Willem Eijsvogel, who all started their bachelor at the same time as me, for the good times and Spar visits. Last, but not least, I would like to thank my girlfriend and fellow master student, Claudia Keijzer, for helping me with input for the thesis, as well as vast emotional support.

References

1. AF Cronstedt. *Rön och beskrifning om en obekant bärg art, som kallas Zeolites*. Vetenskapsakademiens Handl. Stock. (1756).
2. Eelco T.C. Vogt, G. T. W. & Abhishek Dutta Chowdhury, B. M. W. *Zeolites and Zeotypes for Oil and Gas Conversion*. Elsevier - Adv. Catal. **58**, 143–314 (2015).
3. Ch. Baerlocher and L.B. McCusker. *Database of Zeolite Structures*. (2018).
4. Fu, D. et al. *Highly Oriented Growth of Catalytically Active Zeolite ZSM-5 Films with a Broad Range of Si/Al Ratios*. *Angew. Chemie - Int. Ed.* (2017). doi:10.1002/anie.201704846
5. Frantz, T. S., Ruiz, W. A., Da Rosa, C. A. & Mortola, V. B. *Synthesis of ZSM-5 with high sodium content for CO₂ adsorption*. *Microporous Mesoporous Mater.* **222**, 209–217 (2016).
6. Losch, P. et al. *Proton Mobility, Intrinsic Acid Strength, and Acid Site Location in Zeolites Revealed by Varying Temperature Infrared Spectroscopy and Density Functional Theory Studies*. (2018). doi:10.1021/jacs.8b11588
7. Haw, J. F. *Zeolite acid strength and reaction mechanisms in catalysis*. *Phys. Chem. Chem. Phys.* **4**, 5431–5441 (2002).
8. Smit, B. & Maesen, T. L. M. *Towards a molecular understanding of shape selectivity*. *Nature* **451**, 671–678 (2008).
9. Csicsery, S. M. *Shape-selective catalysis in zeolites*. *Zeolites* **4**, 116–126 (1984).
10. Kubarev, A. V. et al. *Solvent Polarity-Induced Pore Selectivity in H-ZSM-5 Catalysis*. *ACS Catal.* **7**, 4248–4252 (2017).
11. Opanasenko, M. V., Roth, W. J. & Čejka, J. *Two-dimensional zeolites in catalysis: current status and perspectives*. *Catal. Sci. Technol.* **6**, 2467–2484 (2016).
12. Choi, J., Ghosh, S., Lai, Z. & Tsapatsis, M. *Uniformly a-oriented MFI zeolite films by secondary growth*. *Angew. Chemie - Int. Ed.* **45**, 1154–1158 (2006).
13. Lai, Z., Tsapatsis, M. & Nicolich, J. P. *Siliceous ZSM-5 Membranes by Secondary Growth of b-Oriented Seed Layers*. *Adv. Funct. Mater.* **14**, 716–729 (2004).
14. Eroglu, N., Emekci, M. & Athanassiou, C. G. *Applications of natural zeolites on agriculture and food production*. *J. Sci. Food Agric.* **97**, 3487–3499 (2017).
15. Stöcker, M. *Gas phase catalysis by zeolites*. *Microporous Mesoporous Mater.* **82**, 257–292 (2005).
16. Vogt, E. T. C., Whiting, G. T., Chowdhury, A. D. & Weckhuysen, B. M. *Zeolites and Zeotypes for Oil and Gas Conversion*. *Advances in catalysis* (2015). doi:10.1016/bs.acat.2015.10.001
17. Janshekar, H., Inoguchi, Y. & Greiner, E. *Chemical Economics Handbook Zeolites*. (2013).
18. Degnan, T. F. *Applications of zeolites in petroleum refining*. *Topics in Catalysis* **13**, (2000).
19. Vogt, E. T. C. & Weckhuysen, B. M. *Fluid catalytic cracking: recent developments on the grand old lady of zeolite catalysis*. *Chem. Soc. Rev.* **44**, 7342–7370 (2015).
20. Zholobenko, V., Garforth, A., Bachelin, F. & Dwyer, J. *Pt/zeolite catalysts for hydrocracking: A comparative study on FAU and EMT*. *Stud. Surf. Sci. Catal.* **105**, 917–924 (1997).
21. Mooiweer, H. H., de Jong, K. P., Kraushaar-Czarnetzki, B., Stork, W. H. J. & Krutzen, B. C. H. *Skeletal isomerisation of olefins with the zeolite Ferrierite as catalyst*. *Stud. Surf. Sci. Catal.* **84**, 2327–2334 (1994).
22. Argauer, R. J. United States Patent Office CRYSTALLINEZEOLITE ZSM-5 AND METHOD OF PREPARING THE SAME assignors to Mobil Oil Corporation No Drawing. Continuation-in-part of abandoned applica. **993**, (1967).
23. Khare, R., Millar, D. & Bhan, A. *A mechanistic basis for the effects of crystallite size on light olefin selectivity in methanol-to-hydrocarbons conversion on MFI*. *J. Catal.* **321**, 23–31 (2015).
24. Li, C. et al. *Selective Introduction of Acid Sites in Different Confined Positions in ZSM-*

- 5 and Its Catalytic Implications. *ACS Catal.* **8**, 7688–7697 (2018).
25. Ristanovic, Z., Kubarev, A. V., Hofkens, J., Roeyffers, M. B. J. & Weckhuysen, B. M. Single Molecule Nanospectroscopy Visualizes Proton-Transfer Processes within a Zeolite Crystal. *Journal of the American Chemical Society* doi:10.1021/jacs.6b06083
 26. Fu, D. et al. Supporting Information Highly Oriented Growth of Catalytically Active Zeolite ZSM-5 Films with a Broad Range of Si / Al Ratios. *Angew. Chemie - Int. Ed.*
 27. Schoonheydt, R. A. UV-VIS-NIR spectroscopy and microscopy of heterogeneous catalysts. *Chem. Soc. Rev.* **39**, 5051–5066 (2010).
 28. Yu, S. Y., Garcia-Martinez, J., Li, W., Meitzner, G. D. & Iglesia, E. Kinetic, infrared, and X-ray absorption studies of adsorption, desorption, and reactions of thiophene on H-ZSM5 and Co/H-ZSM5. *Phys. Chem. Chem. Phys.* **4**, 1241–1251 (2002).
 29. Whiting, G. T. et al. Selective staining of Brønsted acidity in zeolite ZSM-5-based catalyst extrudates using thiophene as a probe. *Phys. Chem. Chem. Phys.* **16**, 21531–21542 (2014).
 30. Valencia, D., Whiting, G. T., Bulo, R. E. & Weckhuysen, B. M. Protonated thiophene-based oligomers as formed within zeolites: understanding their electron delocalization and aromaticity. *Phys. Chem. Chem. Phys.* **18**, 2080–2086 (2016).
 31. Yarulina, I., Chowdhury, A. D., Meirer, F., Weckhuysen, B. M. & Gascon, J. Recent trends and fundamental insights in the methanol-to-hydrocarbons process. *Nat. Catal.* **1**, (2018).
 32. Mores, D., Kornatowski, J., Olsbye, U. & Weckhuysen, B. M. Coke Formation during the Methanol-to-Olefin Conversion: In Situ Microspectroscopy on Individual H-ZSM-5 Crystals with Different Brønsted Acidity. *Chem. - A Eur. J.* **17**, 2874–2884 (2011).
 33. Sun, Q., Xie, Z. & Yu, J. The state-of-the-art synthetic strategies for SAPO-34 zeolite catalysts in methanol-to-olefin conversion. *Natl. Sci. Rev.* **5**, 542–558 (2018).
 34. Jenkins, S. WORLD'S LARGEST SINGLE-TRAIN METHANOL-TO-OLEFINS PLANT NOW OPERATING. *Chemical Engineering, essentials for the CPI professional* (2018). Available at: <https://www.chemengonline.com/worlds-largest-single-train-methanol-to-olefins-plant-now-operating/>.
 35. Dusselier, M. & Davis, M. E. Small-Pore Zeolites: Synthesis and Catalysis. *Chem. Rev.* **118**, 5265–5329 (2018).
 36. Chen, J. et al. Regulation of Framework Aluminum Siting and Acid Distribution in H-MCM-22 by Boron Incorporation and Its Effect on the Catalytic Performance in Methanol to Hydrocarbons. *ACS catalysis* (2016). doi:10.1021/acscatal.5b02862
 37. Xu, S. et al. Advances in Catalysis for Methanol-to-Olefins Conversion. *Advances in Catalysis* **61**, (Academic Press, 2017).
 38. Olsbye, U. et al. Conversion of methanol to hydrocarbons: How zeolite cavity and pore size controls product selectivity. *Angew. Chemie - Int. Ed.* **51**, 5810–5831 (2012).
 39. Nordvang, E., Borodina, E., Ruiz-Martínez, J., Fehrmann, R. & Weckhuysen, B. M. Effects of Coke Deposits on the Catalytic Performance of Large Zeolite H-ZSM-5 Crystals during Alcohol-to-Hydrocarbon Reactions as Investigated by a Combination of Optical Spectroscopy and Microscopy. *Chemistry—A European Journal* **21.48** (2015): 17324–17335
 40. Khare, R. & Bhan, A. Mechanistic studies of methanol-to-hydrocarbons conversion on diffusion-free MFI samples. *J. Catal.* **329**, 218–228 (2015).
 41. Bleken, F. L. et al. Conversion of methanol into light olefins over ZSM-5 zeolite: Strategy to enhance propene selectivity. *Appl. Catal. A Gen.* **447–448**, 178–185 (2012).
 42. Zhang, M. et al. Changing the balance of the MTO reaction dual-cycle mechanism: Reactions over ZSM-5 with varying contact times. *Chinese J. Catal.* **37**, 1413–1422 (2016).
 43. Ilias, S., Khare, R., Malek, A. & Bhan, A. A descriptor for the relative propagation of the aromatic- and olefin-based cycles in methanol-to-hydrocarbons conversion on H-ZSM-5. *J. Catal.* **303**, 135–140 (2013).
 44. Ilias, S. & Bhan, A. Tuning the selectivity of methanol-to-hydrocarbons conversion on

- H-ZSM-5 by co-processing olefin or aromatic compounds*. *J. Catal.* **290**, 186–192 (2012).
45. Mores, D. et al. *Space- and Time-Resolved In-situ Spectroscopy on the Coke Formation in Molecular Sieves: Methanol-to-Olefin Conversion over H-ZSM-5 and H-SAPO-34*. *Chem. - A Eur. J.* **14**, 11320–11327 (2008).
 46. Goetze, J., Yarulina, I., Gascon, J., Kapteijn, F. & Weckhuysen, B. M. *Revealing Lattice Expansion of Small-Pore Zeolite Catalysts during the Methanol-to-Olefins Process Using Combined Operando X-ray Diffraction and UV–vis Spectroscopy*. *ACS Catal.* 2060–2070 (2018). doi:10.1021/acscatal.7b04129
 47. Ramasamy, K. K., Zhang, H., Sun, J. & Wang, Y. *Conversion of ethanol to hydrocarbons on hierarchical HZSM-5 zeolites*. *Catal. Today* **238**, 103–110 (2014).
 48. Sousa, Z. S. B., Veloso, C. O., Henriques, C. A. & Teixeira Da Silva, V. *Ethanol conversion into olefins and aromatics over HZSM-5 zeolite: Influence of reaction conditions and surface reaction studies*. *Journal Mol. Catal. A, Chem.* **422**, 266–274 (2016).
 49. Karthikeyan K. Ramasamy, Yong Wanga, b. *Catalyst activity comparison of alcohols over zeolites*. *J. Energy Chem.* (2013).
 50. Chowdhury, A. D., Paioni, L., Whiting, G. T., Fu, D. & Weckhuysen, B. M. *Unraveling the Homologation Reaction Sequence of the Zeolite- Catalyzed Ethanol-to-Hydrocarbon Process*. *Angewandte Chemie International ed.* (2019).
 51. Weckhuysen, B. M. *Chemical Imaging of Spatial Heterogeneities in Catalytic Solids at Different Length and Time Scales*. *Angew. Chemie Int. Ed.* **48**, 4910–4943 (2009).
 52. Bonilla, G. et al. *Zeolite (MFI) Crystal Morphology Control Using Organic Structure-Directing Agents*. *Chem. Mater.* **382**, 5697–5705 (2004).
 53. Pham, T. C. T., Kim, H. S. & Yoon, K. B. *Supporting Online Material for Growth of Uniformly Oriented Silica MFI and BEA Zeolite Films on Substrates*. *Science (80-.)*. **334**, (2011).
 54. Weckhuysen, B. M. *In-situ Spectroscopy of Catalysts*. *In-situ Spectrosc. Catal.* 1–12 (2004). doi:10.1002/chin.200523297
 55. Pham, T. C. T. et al. *Growth of Uniformly Oriented Silica MFI*. *Science (80-.)*. **334**, 1533–1538 (2011).
 56. Choi, J., Ghosh, S., King, L. & Tsapatsis, M. *MFI zeolite membranes from a- and randomly oriented monolayers*. *Adsorption (2006)*. doi:10.1007/s10450-006-0564-y
 57. Choi, S. Y., Lee, Y.-J., Park, Y. S., Ha, K. & Yoon, K. B. *Monolayer Assembly of Zeolite Crystals on Glass with Fullerene as the Covalent Linker*. *American chemical society (2000)*. doi:10.1021/ja000113i
 58. Kim, E., Choi, J. & Tsapatsis, M. *On defects in highly a-oriented MFI membranes*. *Microporous Mesoporous Mater.* **170**, 1–8 (2013).
 59. Fu, D. et al. *Uniformly Oriented Zeolite ZSM-5 Membranes with Tunable Wettability on a Porous Ceramic*. *Angew. Chemie Int. Ed.* (2018). doi:10.1002/anie.201806361
 60. Park, S. et al. *Acidic and catalytic properties of ZSM-5 zeolites with different Al distributions*. *Catal. Today* **303**, 64–70 (2018).
 61. Ji, M. et al. *Catalytic performances of b-oriented bi-layered HZSM-5 coatings for cracking of hydrocarbon fuels*. *Appl. Catal. A Gen.* **482**, 8–15 (2014).
 62. Cozens, F. L. et al. *Photochemical and Thermal Behavior of Styrenes within Acidic and Nonacidic Zeolites. Radical Cation Versus Carbocation Formation*. *The Journal of Physical Chemistry B* (1997)
 63. Valencia, D. *Elucidating the structure of light absorbing styrene carbocation species formed within zeolites*. *Phys. Chem. Chem. Phys.* **19**, 15050–15058 (1505).
 64. Wulfers, M. J. & Jentoft, F. C. *The Role of Cyclopentadienium Ions in Methanol-to-Hydrocarbons Chemistry*. *ACS Catal.* **4**, 3521–3532 (2014).
 65. Qian, Q. et al. *Single-Particle Spectroscopy on Large SAPO-34 Crystals at Work: Methanol-to-Olefin versus Ethanol-to-Olefin Processes*. *Chem. - A Eur. J.* **19**, 11204–11215 (2013).
 66. Whiting, G. T., Nikolopoulos, N., Nikolopoulos, I., Chowdhury, A. D. & Weckhuysen, B.

- M. Visualizing pore architecture and molecular transport boundaries in catalyst bodies with fluorescent nanoprobe*. Nat. Chem. (2018). doi:10.1038/s41557-018-0163-z
67. Gaag, F. J. Van Der. *ZSM-5 type zeolites : Synthesis and use in gasphase reactions with amonia*. Dissertation 1–112 (1987).